Environmental Science: Atmospheres

ROYAL SOCIETY OF CHEMISTRY

PAPER

View Article Online
View Journal | View Issue

Open Access Article. Published on 20 January 2025. Downloaded on 3/14/2025 3:37:55 PM.
This article is licensed under a Creative Commons Attribution 3.0 Unported Licence.

Check for updates

Cite this: *Environ. Sci.: Atmos.*, 2025, **5**, 348

Particles emitted from smouldering peat: size-resolved composition and emission factors†

Amy L. Wilson,[a] Wuquan Cui,[b] Yuqi Hu,[bc] Marta Chiapasco,[d] Guillermo Rein,[b] Alexandra E. Porter,[d] Geoff Fowler[a] and Marc E. J. Stettler *[a]

Peat fires emit large quantities of particles and gases, which cause extensive haze events. Epidemiological studies have correlated wildfire smoke inhalation with increased morbidity and mortality. Despite this, uncertainties surrounding particle properties and their impact on human health and the climate remain. To expand on the limited understanding this laboratory study investigated the physicochemical characteristics of particles emitted from smouldering Irish peat. Properties investigated included number and mass emission factors (EFs), size distribution, morphology, and chemical composition. Fine particles with a diameter less than 2.5 μm ($PM_{2.5}$), accounted for 91 ± 2% of the total particle mass and the associated mass EF was 12.52 ± 1.40 g kg^{-1}. Transmission electron microscopy imaging revealed irregular shaped metal particles, spherical sulfate particles, and carbonaceous particles with clusters of internal particles. Extracted particle-bound metals accounted for 3.1 ± 0.5% of the total particle mass, with 86% of the quantified metals residing in the fraction with a diameter less than 1 μm. Redox active and carcinogenic metals were detected in the particles, which have been correlated with adverse health effects if inhaled. This study improves the understanding of size-resolved particle characteristics relevant to near-source human exposure and will provide a basis for comparison to other controlled and natural peatland fires.

Received 2nd September 2024
Accepted 17th January 2025

DOI: 10.1039/d4ea00124a

rsc.li/esatmospheres

Environmental significance

Peat fires are some of the largest wildfires on Earth and their emissions lead to extensive regional haze events. Knowledge of the emitted particles' physicochemical properties in relation to climate forcing characteristics, and the causal mechanisms for adverse health effects, remains limited. In this study, emission factors (mass- and number-weighted) and the size-resolved chemical composition of particles emitted during laboratory peat smouldering fires were evaluated. The results find high levels of particle pollution, alongside metals being more abundant in the fine particle fraction that the coarse fraction. This may be of concern for regional air quality. This study provides peat fire emission characteristics for the use in future work on particle exposure health effects and atmospheric modelling studies.

1 Introduction

Annual increases in the Earth's surface temperatures and extreme weather events have been linked with the escalation of wildfires in America, central Asia, and southern Europe.[1–4] One of the most vulnerable wildlands to fire, when drained for agricultural purposes or because of global warming, is peatland.[5,6] Peat is a heterogeneous mixture of slowly decomposing plant material that accumulates in an anaerobic water-saturated environment.[7,8] Peatlands cover around 3% of global land area whilst storing nearly a third of the territorial carbon.[9,10] The fires can have both flaming and smouldering combustion dynamics, with the predominant form being smouldering. Smouldering fires are slow, flameless forms of burning that involve drying, pyrolysis and oxidation of the generated char phases.[11–13] Peat fires can consume more than two orders of magnitude greater fuel than flaming fires per surface area burnt, and burn for extensively long burn periods, often lasting many days or months.[1,7,14]

Literature, to date, has focused on the gaseous emissions from peat wildfires.[15] The wildfires are known to emit hazardous air pollutants, such as formaldehyde, benzene, and poly-aromatic hydrocarbons (PAHs).[16–18] Global carbon dioxide (CO_2) emissions from peat wildfires is equivalent to more than 10% of the global anthropogenic CO_2 emissions per year.[10,19,20] Particles are emitted directly from peat wildfires and are also formed through gas-to-particle conversions in the smoke plume.[15]

[a]Department of Civil and Environmental Engineering, Imperial College London, London, UK. E-mail: m.stettler@imperial.ac.uk

[b]Department of Mechanical Engineering, Imperial College London, London, UK

[c]Sichuan Fire Research Institution of Ministry of Emergency Management of China, Chengdu, China

[d]Department of Materials, Imperial College London, London, UK

† Electronic supplementary information (ESI) available. See DOI: https://doi.org/10.1039/d4ea00124a

© 2025 The Author(s). Published by the Royal Society of Chemistry

Open Access Article. Published on 20 January 2025. Downloaded on 3/14/2025 3:37:55 PM.
This article is licensed under a Creative Commons Attribution 3.0 Unported Licence.

However, research on the toxicity and physicochemical characteristics of the particles emitted from peatland wildfires is limited. There are only a few ambient (inclusive of field *in situ* and *ex situ* measurements, and aircraft campaigns)[21–31] and laboratory studies that evaluate the particle emissions from the smouldering of peat.[18,32–37] Therefore, the causal relationship between the particle properties and the health consequences of inhalation are largely unknown, even though studies have indicated fire haze events can result in increased regional hospital attendance, acute bronchitis, morbidity and mortality.[38–40]

Monitoring peatland fires in the field provides representative measurements but can be challenging due to remote locations, the size of the burns, and highly variable environmental conditions. Additionally, capturing the fire dynamics requires extensive monitoring periods. Proxies for the combustion dynamics, such as the modified combustion efficiency (MCE – the ratio of CO_2 emitted to the sum of carbon monoxide (CO) and CO_2) are not consistently reported and the peat mass loss rate (MLR) is not quantifiable in field studies.[15] Field studies can also be impacted by the sampling environment; specifically, aspects such as particle aging within the plume.[41] Consequently, the ability to compare emissions between field studies is limited.

In contrast, controlled laboratory experiments enable the isolation and investigation of specific peat combustion variables, such as moisture content, burn temperature and inorganic content, and their impact on fire dynamics and emissions.[18,42–47] Laboratory experiments have also provided frameworks for the peat smouldering progression which include ignition, growth, steady, and burn-out stages.[18] The combustion stages are determined through the monitoring of CO_2 and CO emissions, temperature profiles, and MLR: the measurements show very little variation during the steady stage of the fire.[18] Correlating the combustion dynamics with the concentration and composition of the emitted gaseous species and particles is important to understand and compare the toxicity of peatland wildfires across the world.

Furthermore, the particle size distribution (PSD), particularly in terms of particle mass and number emissions, is an important parameter for governing the particle deposition and clearance mechanisms in the body, as well as the inflammation and cardiac effects of the emitted particles.[48–50] Particle number metrics alongside mass metrics are needed because ultrafine particles (UFP, particles less than 100 nm in diameter) contribute very little to the particle mass concentration (PMC), whilst they do contribute significantly to the total particle number concentration (PNC).[51] Particles in the ultrafine range can deposit deeper in the lungs than coarse particles and can cross the air–blood barrier,[52] which may lead to varying biological responses in comparison to exposure to particles with diameters less than 2.5 and 10 μm ($PM_{2.5}$ and PM_{10}).[48,49,53–56] Additionally, *ex vivo* and epidemiological studies have correlated the UFP fraction emitted from smouldering fires with pro-inflammatory responses, increased reactive oxygen species production, and decreased cardiac function.[48,57]

The mass- and number-weighted PSD depend on the biomass type and the combustion dynamics,[37,58–60] however the existing data is still very limited. Literature for peat fires has predominantly focused on the mass concentration of $PM_{2.5}$, rather than considering the PSD.[22,32,35,61,62] To date, number-weighted PSD and number emission factors (EF_N) have not been extensively measured for peat fires compared to mass-weighted EFs (the particle number or mass emitted per unit mass of dry fuel that is burnt).[15,22,24,25,32] Number concentrations were previously presented for ambient particle emissions from a peatland fire, but the combustion dynamics were unknown.[62]

Previous wood burning literature has found that smouldering combustion dynamics, or slower burning, led to a smaller number concentration of particles with a diameter less than 1 μm (PM_1) than for higher temperature or faster burning fires.[59,60,63] The opposite correlation was observed for mass concentration, a higher PMC was found for smouldering fires.[59,60,63] Consequently, to understand the health risks associated with the full range of particles emitted from smouldering-only fires, number and mass metrics should be presented together.[48,50,53]

Additionally, there are only a limited number of studies that evaluate number-weighted PSD measured using different instruments. The existing research highlights instrument consistencies for reference aerosols, but variability for more complex particles.[64,65] Particle bounce, particle de-agglomeration, and impactor overloading, as well as the various instruments having different sizing principles, have all been stated as reasons for the disparities.[66–68] Comparison studies for complex particles, including those from peat burning, are therefore required to improve the confidence in particle number weighted data and to inform World Health Organisation (WHO) air quality guidelines.[69]

Studies considering the size-resolved chemical composition of particles emitted from peat fires are limited, but this is vital for understanding particle deposition, removal pathways, and the toxicity of inhaled smouldering particles.[57,70] Laboratory and *in situ* field studies report that organic carbon (OC) is the predominant component of particles emitted from peat fires, ranging from 58 to 89% of the total particle mass.[24,32,35,71] Source apportionment studies also state higher OC concentrations during haze events than for background measurements.[30,62] A series of OC compounds and PAHs have been detected in particle emitted from peatland fires, and exposure to these compounds at concentrations above the WHO guidelines may result in health risks.[24,29,32] Other OC compounds, such as levoglucosan, *n*-alkanes, and organic acids have been analysed for the purposes of source apportioning ambient particles, or to identify a biomarker for peatland fires.[24,30,48,62,72] Metals and ionic species, such as potassium, aluminium, iron, chromium, nitrate, and sulfate have also been detected and quantified for $PM_{2.5}$.[22,29,62,72,73] Bio-available metals, such as Fe, can catalyse the formation of reactive oxygen species, which can induce a variety of inflammatory responses such as cardiovascular diseases.[74–76] Additionally, a previous health risk assessment identified that four or five individuals out of 1000 may be at risk of cancer when exposed to the carcinogenic metals (such as chromium and

Open Access Article. Published on 20 January 2025. Downloaded on 3/14/2025 3:37:55 PM.
This article is licensed under a Creative Commons Attribution 3.0 Unported Licence.

nickel) in $PM_{2.5}$ from peat fires.[29] Health risk assessments have also highlighted the need to consider total, water-soluble, and extractable particle-bound transition metals (in various leaching agents) to understand the health consequences.[77] Thus, additional laboratory-controlled research on the physicochemical composition of the particles emitted from smouldering peat fires is needed to evaluate the possible health implications for inhalation of fresh particles, by taking into consideration the particle's size, composition, and resulting toxicity.

To investigate the toxicity of the particles emitted from peat fires, this study used controlled laboratory experiments to quantify the size-resolved physicochemical properties of particles emitted during smouldering of horticultural Irish peat. The objectives of the study were to: (i) determine the number- and mass-weighted size distributions and total concentration of the particles emitted, (ii) quantify the particle number and mass EFs, (iii) quantify the concentration of organic and elemental carbon, metals, and ionic species in the emitted particles, and (iv) evaluate particle morphology using transmission electron microscopy. Particle size distribution, morphology, and chemical composition were of particular interest because these factors can influence the site of deposition in the lung, and the toxicity of the particles.[78–80] Further details that aren't included in the main text can be found in the ESI,† where referenced.

2 Materials and methods

2.1 Peat samples

A commercial peat (Shamrock Irish horticultural moss peat, Bord na Mona Horticulture Ltd) was used because of its uniform properties and consistency between batches which ensured experimental reproducibility.[81] The moisture content (MC, mass of water divided by dry peat mass) varies greatly in peatlands and is the single most important factor for ignition.[12,82] Therefore, the MC was maintained at 100%, using a previously described protocol,[18,81] to represent natural conditions whilst also ensuring the successful ignition of the peat. The peat density was 300.0 ± 7.5 kg m^{-3}, and the carbon/hydrogen/nitrogen fractions of the dry peat were 50.21 ± 1.36%, 5.14 ± 0.18%, 1.65 ± 0.82%, respectively.[18,83]

2.2 Smouldering peat fires

The peat samples were burned in an open reactor under controlled conditions, as shown in Fig. 1 and previously outlined in literature.[18,44] Briefly, the sample was ignited using a heated coil along one side of the reactor at 5 cm depth and applying a 100 W power source to the coil until the mass measured by the balance decreased by 10%. The emissions were collected using an inverted fume extraction hood and were transported into a duct with a fan-controlled flow rate (0.034 m^3 s^{-1} ± 2.5%). Four different diagnostic tools were taken during the experiments to monitor the smouldering dynamics: peat mass loss (resolution of 0.01 g), peat temperature profile (twelve K-type thermocouples), infrared imaging of the fire surface spread (FLIR Camera), and real-time concentration of 20 different gaseous species (Nicolet iG50 Fourier-transform infrared spectrometer, Thermo Scientific). The gaseous emissions have previously been reported.[18]

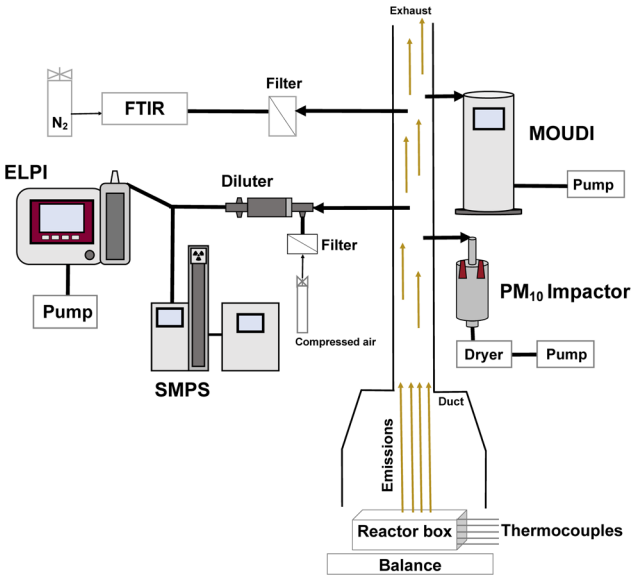

Fig. 1 Schematic of the smouldering peat fire experiment and the instruments used to collect particles by cascade impaction and take real-time measurements of the particle number-weighted size distribution. Note, this schematic does not include diagnostics used for measuring the combustion dynamics.[18]

The experiment protocol was repeated 12 times to quantify various particle physicochemical properties (see Tables 1 and S-1 in the ESI,†) and the repeatability of the particle emissions. The combustion dynamics and particle emission results will be presented as the mean of the experiment measurements, with uncertainty quantified as the standard error of the experiment results. A comprehensive description of the particle measurements, collection procedures, and offline chemical analysis is provided below.

2.3 Combustion dynamics

The combustion dynamics for the laboratory peat smouldering experiment comprise four stages of burning: ignition, growth stage, steady stage, and burn out.[18,84] An example of the combustion dynamic profiles, including MLR, CO_2 and CO, is presented in Fig. S-1 in the ESI.† During the ignition stage the mass loss rate increased to a maximum (0.03–0.04 g s^{-1}), before declining in the growth stage (as the peat fire propagates away from the coil) to 0.02 g s^{-1}. Between 20% and 80% sample mass loss (known as the steady stage, when the mass loss rate is ~0.02 g s^{-1}), the laboratory fire propagation is the most representative of smouldering fire spread in the field and, unlike the ignition phase, is least affected by the ignition coil.[9,44] For these reasons, only the results from the steady stage are presented in this paper.

Table 2 includes data used to monitor combustion dynamics during the steady stage. The average MCE value was consistent with literature values for smouldering fires (MCE – 0.65 to 0.85), and below the value for flaming-only fires (0.99).[15,41,47] The average peak temperature and spread rate were also consistent

 © 2025 The Author(s). Published by the Royal Society of Chemistry

Open Access Article. Published on 20 January 2025. Downloaded on 3/14/2025 3:37:55 PM.
This article is licensed under a Creative Commons Attribution 3.0 Unported Licence.

Table 1 Summary of particle collection methods and the physicochemical analysis undertaken to determine the particles' characteristics

Instrument or sampler	Particle size range/μm	Particle sample physical analysis	Chemical analysis technique	Chemical analysis
Scanning mobility particle sizer (SMPS)	0.016–0.550	PNC & PSD		
Electrical low-pressure impactor (ELPI)	0.006–10 (14 stages)	PNC & PSD		
Micro-orifice uniform distribution impactor (MOUDI)	0–9.9 (13 stages)	PMC & PSD		
Dekati PM_{10} impactor	0–10 (3 stages)	PMC & PSD	Ion chromatography (IC) and inductively-coupled plasma-optical emission spectroscopy (ICP-OES)	Ionic, low molecular weight acids, and elemental composition
Thermophoresis sampler	All particles (1 stage)	Morphology	Energy-dispersive X-ray spectroscopy (EDS) and Raman spectroscopy	Elemental composition
Filter collection using sampling pump	All particles		Organic carbon/elemental carbon instrument	Total, organic, and elemental carbon

Table 2 Average combustion dynamic parameters for the smouldering Irish peat experiments

Peat	Spread rate/cm h^{-1}	Mass loss rate/g s^{-1}	Modified combustion efficiency	Peak temperature/°C
Irish (H)	1.17 ± 0.11	0.0211 ± 0.0022	0.860 ± 0.011	578.93 ± 36.30

with other smouldering studies; smouldering combustion is low-temperature, peaking at around 500 to 700 °C, and slow spreading (1 to 3 cm h^{-1}) relative to flaming combustion of peat, where temperatures reach 1500 to 1800 °C and spreading is two orders of magnitude faster.[7]

2.4 Particle concentration and size distribution

Two real-time measurement instruments were used to determine the particle size distribution and number concentration. The Scanning Mobility Particle Sizer (SMPS, Model 3938, TSI Inc) and the Electrical Low-Pressure Impactor (ELPI+™, Dekati Ltd) were used in parallel, as shown in Fig. 1, to measure the particle size distributions between 6 nm and 10 μm. An ejector diluter (L7 Diluter, Dekati Ltd) was placed in line with the duct prior to the SMPS and ELPI, to dilute the air by 8 : 1.

The SMPS consisted of a long Differential Mobility Analyser (DMA, Model 3081A, TSI Ltd), a Condensation Particle Counter (CPC, Model 3756, TSI Inc), and a neutraliser (Model 3088, TSI Ltd). It was operated with a sheath flow of 3 L min^{-1} and the CPC flow rate at 0.3 L min^{-1}. Particles with diameters between 16 nm and 560 nm were separated according to their electrical mobility diameter (d_m), and their number concentrations were corrected for multiple charge effects and diffusion loss using the in-built SMPS software algorithms. d_m is defined as the diameter of a unit density spherical particle moving at the same velocity in an electric field as the particle in question.[85]

The ELPI was operated at a flow rate of 9.66 ± 0.03 L min^{-1}. The size distribution and number concentrations were collected every second for particles sized between 6 nm and 10 μm. The particles, which were charged by the corona charger, entered the low-pressure cascade impactor, were separated according to their inertia and collected on the 14 sintered plate stages. Particles were classified by their aerodynamic diameter (d_a); the diameter of a unit-density sphere having the same gravitational settling velocity as the particle in question.[85] Additional information on the calculation of the number concentration can be found in the ESI.†

A three-stage PM_{10} Impactor (Dekati Ltd) was used to collect particles for chemical analysis (ionic and metal content) using polycarbonate (25 mm, Nuclepore Track Etch Filter, Whatman) and borosilicate glass microfibers filters (47 mm, Emfab, Pallflex) using a 30 ± 1.5 L min^{-1} flow rate. The three-stages and back-up filter had cut-off points of 10 μm, 2.5 μm, and 1 μm, respectively. Filters were weighed (Sartorius BP211D Basic Plus Analytical Balance, 0.00001 g resolution) to determine the PMC.

A Micro-orifice Uniform Deposition Impactor (MOUDI, MSP, Model 125R) was also used to collect particles for gravimetric analysis using PTFE filters (Fluoropore, 0.45 μm pore size, 47 mm diameter) using a flow rate of 9.5 ± 0.3 L min^{-1}. The thirteen-stages had cut-off points of 9.9, 6.2, 3.1, 1.8, 1.0, 0.56, 0.31, 0.18, 0.1, 0.055, 0.032, 0.018, 0.010 μm. The additional MOUDI stages, in comparison to the PM_{10} Impactor, provided additional insights into the particle mass-weighted size distribution, as well as the contribution from the UFP fraction.

The uncertainty in the particles mass measurements for the MOUDI and Dekati PM_{10} Impactor samples were estimated by propagating the standard deviation of the triplicate measurements of pre- and post-sampling filter mass and the standard deviation in the instruments flow rate, as presented in Tables S-2 and S-3.† The analytical uncertainty was less than the

Open Access Article. Published on 20 January 2025. Downloaded on 3/14/2025 3:37:55 PM. This article is licensed under a Creative Commons Attribution 3.0 Unported Licence.

standard error, so we report the latter for all gravimetric and chemical analyses.

2.5 Morphology, particle size, and elemental composition

Particles were collected on 300-mesh copper transmission electron microscope (TEM) grids coated with a lacey carbon supporting film using a thermophoretic sampler set at 5 V (DC), with a flow rate of 0.3 L min^{-1}.[86]

Particle size, shape, and the composition of 60 individual particles that had a Feret diameter of less than 10 μm were analysed using a Jeol 2100Plus Scanning TEM (STEM, Jeol Ltd, UK) coupled with an energy dispersive spectroscopy (EDS) instrument (X-max 80T Aztec detector, Oxford Instruments). The TEM was operated at 200 kV, whilst the elemental maps were acquired for 30 minutes with a 15° solid angle using EDS. Particles with a diameter greater than 10 μm were not analysed.

2.6 Particle chemical composition analysis

Extractable metals: a closed vessel microwave digestion system (Multiwave 3000, MF100 drum, Anton Parr) was used for the digestion and extraction of elements from the particle samples collected using the PM_{10} Impactor (cut-off points of 10, 2.5, and 1 μm). Prior to their use, the microwave vessels were soaked overnight in 10% nitric acid (HNO_3) to remove any contamination. The microwave protocol was adapted from previously validated methods that are stated in literature.[87] Briefly, half of each filter underwent HNO_3 (68%) microwave digestion. The microwave was set to 3 min ramp to 95 °C, 5 min hold, 3 min ramp 120 °C, 5 min hold, 3 min ramp to 130 °C, and 2 min hold to extract the elements. A diluted extracted solution was filtered through a 0.45 μm cellulose membrane filter prior to being analysed by ICP-OES (Avio 500, PerkinElmer) for the determination of the concentrations of 18 elements: Al, B, Bi, Ba, Cd, Co, Cr, Cu, Fe, Mg, In, Ga, Mn, Ni, K, Sr, Pb, and Zn. The concentration of the metals is presented as an average of the nine collections with their associated standard error. The limit of detection and quantification for each element is shown in Table S-4.† Certain elements, such as B, Bi, Pb, Ni, In, Cu, Co, and Mn were not detected, or their concentration were below the quantification limit.

Particle ionic content was determined by Ion Chromatography (IC) (Dionex ICS-2100, Thermo Scientific). The ionic species were extracted from half of each filter (PM_{10} Impactor filters) using 10 mL of 18.2 MΩ ultrapure water and ultrasonic agitation for 1 h.[62] The extract was subsequently filtered through a 0.45 μm cellulose membrane filter and analysed for K^+, Ca^{2+}, Mg^{2+}, Na^+, Li^+, Br^-, F^-, Cl^-, SO_4^{2-}, PO_4^{3-}, NO_3^-, NH_4^+, and NO_2^-, as well as three low molecular weight acids (oxolate, formate, and acetate). The concentrations of these ions are presented as a mean of the six collections with their associated standard error. The limit of detection and quantification for each element is shown in Table S-5.† Certain ions, including Br^-, PO_4^{3-}, and Li^+, were not detected.

Three blank filter samples, that had been placed in the PM_{10} Impactor prior to any experiments, were also analysed for ionic and metal content.

Organic and elemental carbon: particles were collected on quartz fibre filters (47 mm, Tissuquartz, VWR) for 20 minutes using an air sampling pump (Sidekick, Model 224-52MTX, SKC) at a flow rate of 2 L min^{-1}. The National Physical Laboratory (NPL, UK) then analysed the bulk samples for OC and EC content by taking a 1.5 cm^2 punch of the filter and subjecting the sample to thermal optical analysis using an OC/EC analyser (Organic Carbon/Elemental Carbon Instrument, Model 5 L, Sunset Laboratory Inc). This followed NPL's ISO 17025 accredited in-house procedure QPAS/B/561 using the EUSAAR2 thermal protocol. The uncertainty in the TC measurements is reported as the standard error multiplied 2 (~95% confidence interval), in accordance with NPL's UKAS accreditation.

Particle phase was analysed by Raman Spectroscopy (inVia Raman Microscope, Renishaw). The instrument was equipped with confocal optics and a nitrogen-cooled charge coupled device (CCD) camera detector. The excitation laser beam (confocal mode at 532 nm) was focused on a sample area of ~100 nm, with a final laser power of 0.5 mW (1% of laser power). The acquisition time was 10 s per accumulation, with a total of 5 accumulations per particle sample area. 18 particles were analysed to gain an insight into the sample structural heterogeneity.

2.7 Emission factor calculation

The carbon mass balance approach was used to determine the fuel-based CO_2 EFs, in units of mass of analyte per kilogram of fuel burned, as shown in eqn (1).[88]

$$\mathrm{EF_{CO}} = F_\mathrm{C} \times 1000\left(\mathrm{g\ kg^{-1}}\right) \times \frac{\mathrm{MM_{CO_2}}}{\mathrm{MM_C}} \times \frac{C_\mathrm{X}}{C_\mathrm{T}} \quad (1)$$

where F_C is the mass fraction of carbon in the dry biomass, MM_{CO_2} is the molar mass of CO_2 (g per mole), MM_C is the molar mass of carbon (g per mole), C_X is the number of moles of emitted species (X) and C_T is the total number of moles of carbon emitted (including carbon in gaseous and particulate form).

The peat carbon content ($F_C = 50.21 \pm 1.36\%$) as well as the concentration of carbon detected in the particle and gaseous phases were included in the EF calculations.

The carbon content in the remaining residue after the smouldering experiments was measured using a CHNS elemental analyser (Flashsmart CHNS/O, CE Instruments Ltd). The fraction of carbon remaining in the residue, was found to be approximately 1.5% of the total unburnt peat carbon content. This value was included in the carbon mass balance calculation of the particle mass, particle number, and particle-bound species EFs, as shown in eqn (2).[36,71]

$$\mathrm{EF_X} = F_\mathrm{c} \times \left(1 - X_\mathrm{R,C}\right) \times 1000\left(\mathrm{g\ kg^{-1}}\right) \times \frac{\mathrm{MM_X}}{\mathrm{MM_C}} \times \frac{C_\mathrm{X}}{C_\mathrm{T}} \quad (2)$$

where $X_{R,C}$ is the fraction of fuel carbon that remains in the residue after the burning of peat is complete (no additional mass is lost). CO_2 was then used as a reference species to calculate the particle mass and number EFs, as well as the composition related EFs using the following equation.[24,89]

 © 2025 The Author(s). Published by the Royal Society of Chemistry

Open Access Article. Published on 20 January 2025. Downloaded on 3/14/2025 3:37:55 PM.
This article is licensed under a Creative Commons Attribution 3.0 Unported Licence.

$$EF_X = \frac{\Delta X}{\Delta CO_2} \times EF_{CO_2} \quad (3)$$

where ΔX is the concentration (mass concentration, mg m^{-3} and number concentration, cm^{-3}) of the species X and ΔCO_2 is the concentration of CO_2 (mg m^{-3}).

3 Results

The physicochemical characteristics including size distribution, concentration, morphology, and the chemical composition of particles emitted from the Irish peat smouldering fires were evaluated. The $PM_{2.5}$ fraction accounted for 94 ± 2% of the total particle mass sampled, whilst particles with a diameter less than 560 nm accounted for more than 95% of the total particle number concentration. Particles were also collected for offline analysis of OC, EC, metal, and ionic content. The chemical mass balance was in reasonable agreement with the gravimetric analysis, with a mass deficiency of approximately 19% being attributed to elements not analysed for (such as Si), measurement errors, and water content. The particles emitted from the smouldering peat burns had a high carbon content. The OC mass fraction ranged from 74 to 78% of the total particle mass; however, the EC fraction accounted for less than 0.5% of the total particle mass. These values agree with laboratory and in-plume peat fire studies, including those from temperate, tropical and boreal peat fires, as shown in Table S-6 in the ESI.† The average total quantifiable metal mass accounted for 3.1 ± 0.5% of the total particle mass (PM_{10}), in agreement with previous laboratory and ambient peat fire studies (range 0.07 to 13% of particle mass).[27,29,62,71,90,91] The total quantifiable ionic mass contributed 1.2 ± 0.4% to the total particle mass (excluding ions which were characterised under the metal analysis), whilst the low molecular acids contributed approximately 0.6% of the total particle mass. This average ionic mass value was at the lower end of the range found in literature for particles emitted from peat fires (1–40%).[24,62,92]

The following sections will evaluate the size distribution and size-resolved chemical composition of the particles emitted from the smouldering peat fires.

3.1 Particle mass distribution

The average MOUDI-measured mass-weighted particle size distribution of emitted particles from the smouldering fires is given in Fig. 2, alongside the percentage cumulative mass calculated for both the MOUDI and PM_{10} Impactor measurements. We observe two peaks in the mass-weighted particle size distribution, between 0.32 to 0.55 μm and 1 to 1.8 μm, which is in agreement with previous literature.[92]

The PM_{10}, $PM_{2.5}$, and PM_1 mass concentrations are shown in Table 3. The $PM_{2.5}$ mass concentrations, measured by the MOUDI and PM_{10} impactor, were equivalent to 91 ± 2% and 94 ± 2% of the total particle load, respectively. The large contribution of the $PM_{2.5}$ fraction to the total PM_{10} mass is consistent with existing literature.[15,18,25,48,61] The PM_1 fraction accounted for 69 ± 4% and 65 ± 1% of the $PM_{2.5}$ fraction, for the samples taken using the MOUDI Impactor and the PM_{10} Impactor, respectively.

The average $PM_{2.5}$ EF_M were within the range of existing temperate peat fire measurements in the laboratory (6.6 to 49 g kg^{-1}, $n = 5$).[18,25,32,33,36] To date, only one field study in North Carolina,[25] to the authors knowledge, has quantified $PM_{2.5}$ EF_M. The $PM_{2.5}$ EF_M associated with the North Carolina study stated an EF_M approximately four times larger than this study's measurements for the combustion of Irish peat.

The combustion dynamics resulting from the variations and interactions between the peat density, MC, inorganic content, peat porosity, and carbon content, as well as the ignition protocols and diffusion of heat and oxygen through fuel, may explain the large variation of EF_M presented in the literature.[9,43,47,60,93] Additionally, environmental factors such as the time since the last peat fire or disturbance to the peatland may impact the emissions from the fires.[32]

The differences between the EF_M measured by the MOUDI and PM_{10} Impactor for PM_1, $PM_{2.5}$, and PM_{10} fractions are within the measurement uncertainty. The small discrepancy for particles with a $d_a < 2.5$ μm may be a result of reduced collection efficiency potentially caused by particle bounce and internal losses within the PM_{10} impactor.[85] Furthermore, the rotation of the MOUDI stages, as well as the micro-orifice nozzles, are

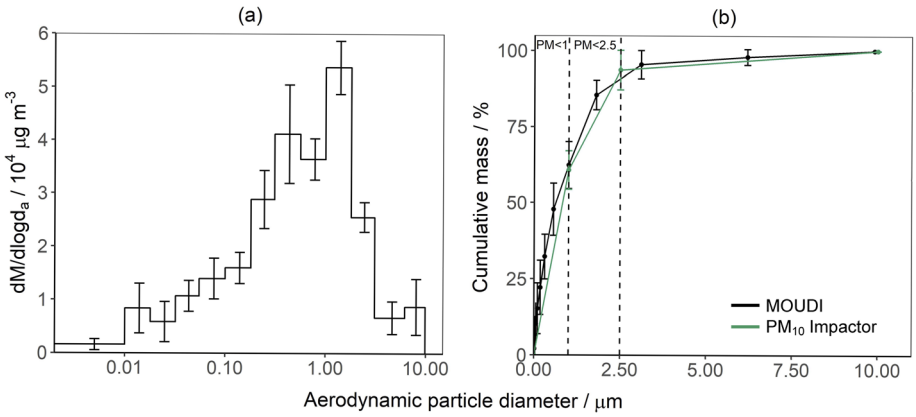

Fig. 2 (a) The average mass-weighted size distribution of particles collected using the MOUDI during the steady stage of burning (20 to 80% of the dry peat mass lost). (b) The average cumulative mass of the particles collected using the PM_{10} Impactor and the MOUDI. Error bars represent ± standard error.

Open Access Article. Published on 20 January 2025. Downloaded on 3/14/2025 3:37:55 PM.
This article is licensed under a Creative Commons Attribution 3.0 Unported Licence.

Table 3 Average mass concentration and emissions factors collected using the PM_{10} Impactor and MOUDI. Errors represent ± standard error where $n = 13$ for PM_{10} Impactor measurements and $n = 6$ for MOUDI measurements

Particle fraction	Instrument	Mass concentration/μg m^{-3}	Mass emission factor/g kg^{-1}
PM_1	PM_{10} impactor	4120 ± 567	8.16 ± 0.98
	MOUDI	4191 ± 761	8.86 ± 1.32
$PM_{2.5}$	PM_{10} impactor	6304 ± 853	12.47 ± 1.44
	MOUDI	5884 ± 810	12.52 ± 1.40
PM_{10}	PM_{10} impactor	6721 ± 916	13.34 ± 1.54
	MOUDI	6541 ± 1000	13.84 ± 1.62

expected to reduce overloading, minimise particle bounce and re-entrainment of particles, as well as minimising losses of semi-volatile and volatile particles.[94] These additional features enabled longer collection times with the MOUDI compared to the PM_{10} Impactor, which enabled the MOUDI to capture more of the variability in the particle emissions over the course of the steady stage of the peat fires.

Nevertheless, due to the inhomogeneity in composition of *in situ* peat (often undisturbed) and the environmental factors impacting fresh particle emissions, these mass metrics cannot be scaled to natural peat fires without a consideration of the combustion dynamics, peat density, composition, and MC.

3.2 Particle number distribution

To date, inter-comparison studies that evaluate the measurement of mass- and number-weighted particle size distribution are limited. Specifically for peat fires, the studies that have measured the number-weighted particle size distribution have not evaluated the same particle size range, leading to large uncertainty when comparing results. This study addressed this by using two near real-time devices, which classify the particles based on different equivalent diameters, and comparing the number size distributions and EF_N.

The normalised number-weighted particle size distributions from the ELPI and SMPS measurements are presented in Fig. 3. The SMPS measurements showed a bimodal distribution with peaks at 60 nm and 150 nm, similar to a previous ambient study,[92] however a bimodal distribution is not consistently observed during biomass haze events.[28]

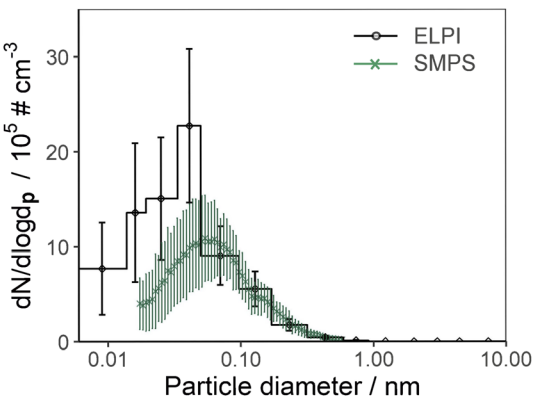

Fig. 3 An example of the number-weighted particle size distribution for the ELPI and the SMPS measurements. Error bars represent ± standard error.

The average GMD for both instruments was in the UFP range (<100 nm), as shown in Table 4. The SMPS derived GMD was in agreement with the limited number of studies that considered the particle number-weighted size distribution (using mobility diameter as the equivalent diameter) for peat fires, as displayed in Table 4. The disparity between the aerodynamic and mobility diameter size distributions (d_a and d_m) was confirmed by instrument checks that showed that the electrical currents measured by all ELPI stages were above the noise limits, all instrument parameters were correct, and appropriate zeroing methods had been followed. The particles emitted from the peat fires are complex in morphology (see Section 3.6), and the particle density is unknown and is likely to vary for particles of different composition. These factors all impact the charging mechanisms within the instruments and the equivalent diameter reported by the ELPI and SMPS.

For example, the particle density may vary as a function of size and therefore, using a single particle density value in the ELPI calculations may not be suitable.[95,96] As the d_a GMD was smaller than the d_m GMD, the emitted particles may have a density less than 1 g cm^{-3}, less dense particles impact on lower stages in the ELPI instrument than an equivalent particle with unit density. Additionally, the particles are not all spherical, which has previously been found to lead to an ELPI size distribution that is broader than the SMPS distribution.[66,97] A previous study also stated a potential mobility diameter peak less than 0.01 μm may exist for particles emitted from peat fires, but because of the size range of the SMPS the peak could not be resolved.[92] Furthermore, the rapidly varying particle emission rates may have exacerbated the small particle correction of the ELPI.[95] Consequently, having both the d_a and d_m measurements provides greater insight into the physical behaviour of the particles.

The smouldering average PNC and EF_N values for measurements with both the ELPI and SMPS are shown in Table 4 alongside existing literature values. This study's average PNCs, determined from the respective instruments, are one or two orders of magnitude greater than those reported from ambient measurements.[28,62] This is mostly likely due to differences in the proximity to the fire and plume dilution processes.

The average EF_N values, shown in Table 4, were in agreement with the singular laboratory study that has considered peat

 © 2025 The Author(s). Published by the Royal Society of Chemistry

Open Access Article. Published on 20 January 2025. Downloaded on 3/14/2025 3:37:55 PM.
This article is licensed under a Creative Commons Attribution 3.0 Unported Licence.

Table 4 Comparison of the particle number emission data from this study and existing literature. For this study, error bars represent ± standard error where $n = 5$ for the SMPS and $n = 7$ for the ELPI measurements

Instrument (particle size range)	Location (peat)	Number concentration/10^5 cm^{-3}	Number emission factor/10^{15} kg^{-1}	GMD/nm	Reference
SMPS (16–560 nm)	Laboratory (Irish)	6.57 (±1.43)	1.49 (±0.16)	74 (±4)	This study
ELPI (0.06–10 μm)		21.90 (±4.76)	4.61 (±0.71)	29 (±3)	This study
CPC (0.01–2.5 μm)	Ambient (Indonesian)	0.21–1.7			See *et al.* (ref. 62)
SMPS and APS (0.008 to 19 μm)	Ambient (Indonesian)	5.31 (±8.33)		Bimodal (50 nm and 400 nm)	See *et al.* (ref. 92)
Fast mobility particle sizer – FPMS (5.6–560 nm)	Ambient (Indonesian)	0.40 (±0.03)		60	Betha *et al.* (ref. 28)
SMPS (15–680 nm)	Laboratory (Florida)	5.38 (±4.17)	2.88 (±2.82)	90	Bhattarai *et al.* (ref. 37)
SMPS (15–680 nm)	Laboratory (Siberian)		6.86 (±3.93)		Bhattarai *et al.* (ref. 37)
	Laboratory (Malaysian)		3.14		

emission factors,[37] and the limited smouldering literature values associated with other types of biomass burning.[60,63,98,99] To date, no field studies have quantified EF_N for smouldering peat fires. The EF_N values will be dependent on the peat type, the ignition protocol, the burn temperature and efficiency, sampling dilution, and particle losses within the sampling system but are expected to be a conservative estimate as our measurements do not account for any atmospheric ageing and secondary organic aerosol nucleation processes.[37]

3.3 Particle carbon content

The high contribution of OC to total carbon (TC) (96 ± 3%) and the OC : EC ratio (range: 181 to 212) are typical for smouldering or low-temperature combustion fires of various biomasses,[24,73,90,100] and are strongly indicative of pyrolysis processes. Conversely, for flaming or mixed phase burns the OC : EC ratio decreases with the increase in EC emissions.[100] The variation in peat type, combustion dynamics, and sampling location, as well as thermal optical method protocols consequently leads to the broad range of OC/EC ratios within the literature, as shown in Table S-6 in the ESI.† Visual inspection of the particle samples on the filters further supports the high OC content: the filters were coated with bright yellow somewhat-oily particles as shown in Fig. S-2 in the ESI.† Additionally, the percentage of OC as a function of the total particle mass (76%) was consistent with values stated in laboratory and field studies as shown in Table S-6 in the ESI.†

3.4 Particle metal content

Metals can be displaced during the combustion of peatlands either through vaporisation or emitted as fly ash particles,[101] however the relatively low proportion of the total particle mass that was attributed to metals (3.1 ± 0.5%), compared to other quantified species such as OC and the ash remaining in the residue, indicated minimal transfer of metals to the particle phase.

Al, Fe, K, and Mg were the most abundant trace metals detected in the particle samples. Together the metals accounted for approximately 85% to the total particle-bound metal mass detected. The high proportion of crustal metals was expected due to the high abundances of the metals in peat core samples, and the potential for alkali metals, present as salts, to be released at the low temperatures associated with smouldering combustion.[102,103] Other trace metals such as Ba, Zn, and Sr were also detected; however, unlike in previous studies,[32,104] toxic metals, such as Pb, and Ni were not detected in the particles collected during this studies' Irish peat fires. The metal content of the particles was also found to be lower than previous studies of flaming, high temperature, burns.[57,105]

In this study, approximately 86% of the total quantified metal content resided in the PM_1 fraction, which aligned with a higher PM_1 mass in comparison to the other particle size fractions. The contribution of individual metals to the PM_1, $PM_{1-2.5}$ and $PM_{2.5-10}$ fractions is shown in Fig. 4. Carcinogenic metals, Cr and Cd, were only detected in the one of the PM_1 samples, whilst Fe was only above the limit of quantification in

Open Access Article. Published on 20 January 2025. Downloaded on 3/14/2025 3:37:55 PM.
This article is licensed under a Creative Commons Attribution 3.0 Unported Licence.

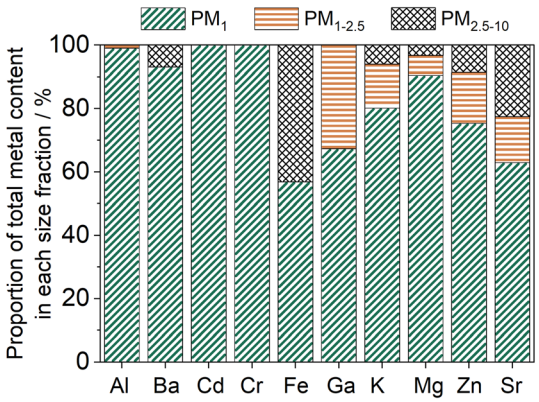

Fig. 4 The proportion of individual metals in the three particle samples relative to the total particle-bound mass of each metal.

three of the nine PM_1 samples. When detected, Fe accounted for around 4% of the PM_1 total metal mass.

The relative contribution of each metal to the total elemental mass has previously been found to vary depending on geographical location of the peat fire, the temperature of the burn, and number of metals analysed for.[36,105]

The size-resolved metal EFs for this study are shown in Fig. 5. The particle-bound metal EFs are in agreement with the limited number of studies that have evaluated elemental EFs.[24,36] Metal EFs, as a function of fuel consumed, are limited in the literature because often CO and CO_2 emissions are not monitored, or the mass of peat burnt in unknown. To date, metal concentrations and ratios (metal concentration as a function of particle mass) are more frequently reported.[24,29,32,62,92,103,106] Other biomass burning studies (including forest, savanna, and crop residue fires) have also stated particle-bound metal EFs of similar magnitude to this study.[41,107]

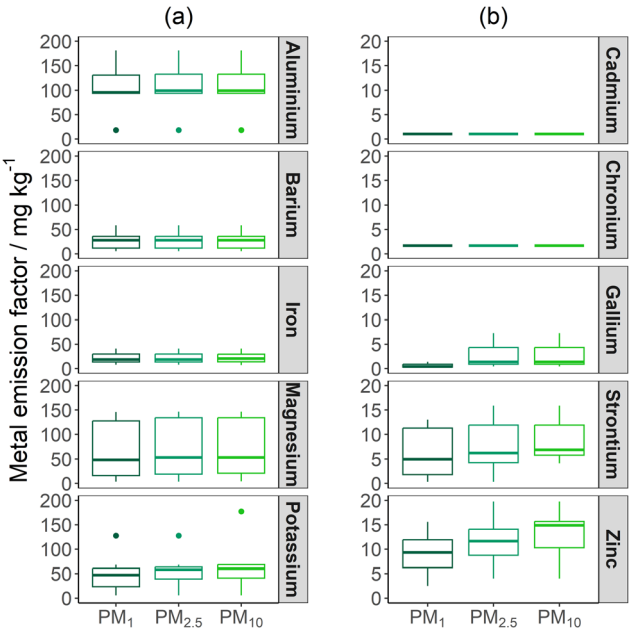

Fig. 5 Boxplot of the particle-bound major (a) and minor (b) trace metal EFs for the Irish peat burns. The lower and upper box boundaries represent 25th and 75th percentiles, respectively, whilst the line inside the box represents the median value. Error lines represent the maximum and minimum data, and filled circles represent data that falls outside the extremes of the boxplot (25th and 75th percentile ± 1.5 × interquartile range).

3.5 Particle ionic content

Sulfate accounted for 18% of the total ionic mass in the PM_{10} fraction, whilst particle bound ions, NH_4^+, K^+, and Na^+, constituted around 31% of the total ionic mass for the collected particles in this study, which is in agreement with existing ambient literature.[33,62,92] Water-soluble Mg and K concentrations were equivalent to less than 80% of the total element concentration detected by ICP-OES.

Size-resolved analysis also identified quantifiable concentrations of water-soluble F^-, Cl^-, and NO_2^- ions, as shown in Fig. 6. The detected ions were found to predominantly reside in the particle samples with a d_a less than 1 μm (89 ± 3% of total ionic concentration). This is in agreement with a previous temperate peat study which identified over half of the ionic species resided in the fine particle fraction.[33] Ions such as NH_4^+, Mg^{2+}, SO_4^{2-} and NO_2^- were also detected in particle samples with a d_a greater than 1 μm, whilst ionic species, such as Na^+, K^+, and Ca^{2+} were only detected in samples with a d_a less than 1 μm, as shown in Fig. 6.

Low molecular weight acids (acetate, oxolate, and formate) accounted for around 0.6% of the total particle mass detected in the particle samples. Acetate and formate accounted for 13 ± 6% and 14 ± 9% of the total ionic mass, whilst oxolate accounted for less than 10% of the total ionic mass. The higher abundance of monocarboxylic acids than the dicarboxylic acid (oxolate) is indicative of predominantly primary combustion emissions.[62,108,109] A larger ratio of oxolate to formate/acetate would have indicated greater levels of secondary photochemistry and liquid-phase oxidation.[110]

The size-resolved particle ionic EFs are shown in Fig. 7. For the first time ionic EFs have been reported for Irish peat burns, and only a limited number of temperate peat fire emission studies have determined the particle ionic EFs. The particle-

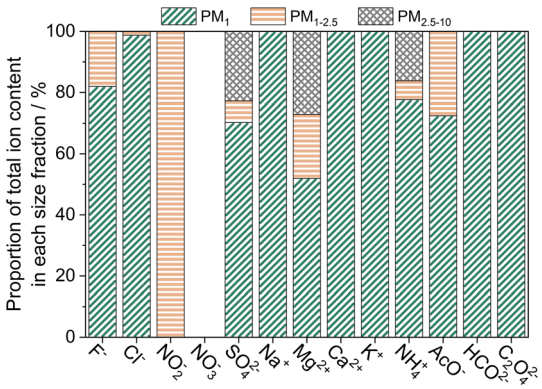

Fig. 6 The proportion of individual ions in the three particle samples relative to the total particle-bound mass of each ion.

 © 2025 The Author(s). Published by the Royal Society of Chemistry

Open Access Article. Published on 20 January 2025. Downloaded on 3/14/2025 3:37:55 PM.
This article is licensed under a Creative Commons Attribution 3.0 Unported Licence.

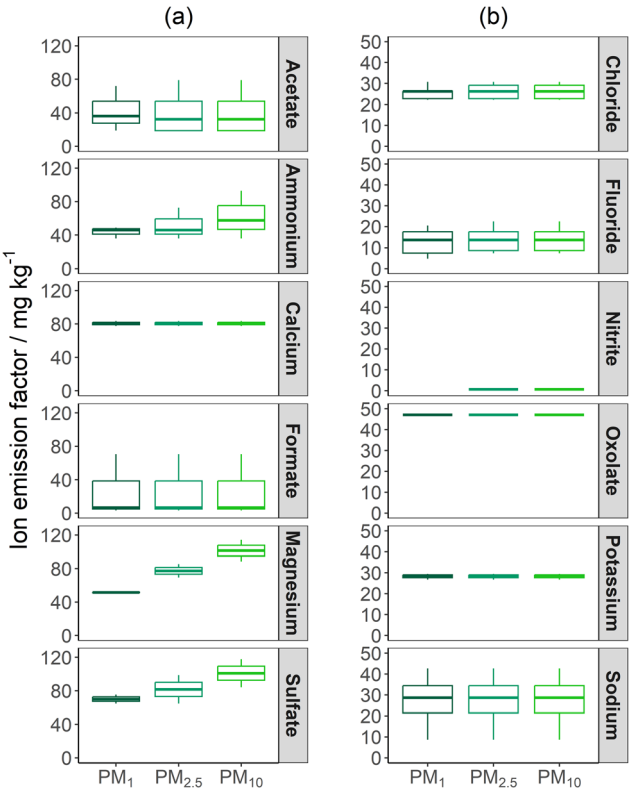

Fig. 7 Boxplot of the particle-bound major (a) and minor (b) ion and low molecular weight acid EFs for the Irish peat burns. The lower and upper box boundaries represent 25th and 75th percentiles, respectively, whilst the line inside the box represents the median value. Error lines represent the maximum and minimum data, and filled circles represent data that falls outside the extremes of the boxplot (25th and 75th percentile ± 1.5 × interquartile range).

bound EFs, in particular Cl^-, NH_4^+, K^+, and SO_4^{2-} EFs, were in agreement with literature values for temperate peat fires.[33]

Other peat fire literature has identified the distribution of ionic species as a function of particle size varies with peat type, geographical location, combustion conditions and aging of plume.[23,33,62] Literature has identified Na^+ and Cl^- as the most abundant ionic species, whilst the proportions of F^-, K^+, SO_4^{2-}, NO_2^-, NO_3^-, Mg^{2+}, and Ca^{2+} ions has shown to vary. Alongside the variations in peat soil and combustion dynamics, the gaseous emissions and gas-to-particle conversion after combustion influence the concentrations of SO_4^{2-}, NH_4^+, and other nitrogen-based ions. Therefore, as the particles were collected close to source in this study the concentrations of SO_4^{2-}, NH_4^+, and other nitrogen ions are likely to be lower than that measured in the ambient environment.

3.6 TEM and Raman analysis

TEM images of the particle samples showed an array of particle sizes; the size distribution of the 60 analysed particles is shown in Fig. S-3 in the ESI.†

The complexity of the particle morphologies and composition are shown in Fig. 8 and 9. EDS maps of the particles in Fig. 8 are shown in Fig. S-4 to S-10 in the ESI.† Many of the particles had irregular and non-spherical morphologies, for example, particles B–F in Fig. 8. Particles A and E in Fig. 8 appeared to spread over the grid, indicating that these particles were hydrated, had a low viscosity, or a low surface tension.[111–113] Particles A and E are consistent with those collected near to biomass fires (fresh samples), whilst aged-smoke particles (further away from fire) have previously been found to be spherical and have become known as tar-balls.[111,113,114] Tarballs are defined in literature as spherical, amorphous, not aggregated with other particles or have inclusions, stable under the electron beam, and are likely form from gas-phase nucleation or secondary processes within the primary particles as the plume ages.[111,113,114]

The particles, shown in Fig. 8, had a varied composition and were composed of a range of different elements, including Al, Fe, Mn, Ca, Ni, K, Zn, S, Cr, and Nd. The composition of the particles in Fig. 8(B and D) was consistent with previous findings of fly ash or mineral dust particles in biomass burning plumes.[115] The presence of metal salts in biomass burning particles, such as potassium sulfate, has also been reported.[113] Organic sulfur is also common in peatland soils,[116] which can be emitted in the form of sulfur dioxide and undergo heterogenous oxidation with nitrogen oxide on the surface of particles to formulate the sulfur-rich particles in Fig. 8(A).[117,118]

Raman spectra, shown in Fig. S-11 in the ESI,† further confirmed the presence of Fe, through the identification of iron oxides such a goethite, ferrihydrite, and haematite. The transformation of these crystal phases is dependent on temperature and pH, and may be catalysed by cations such as Zn and Ni.

The extraction effectiveness of particle-bound metals for ICP-OES analysis was likely dependent on the form Fe was present in, such as iron-oxides or iron-aluminosilicates.[119,120] As a result the total elemental content may not have been detected by ICP-OES analysis, because the HNO_3 extraction protocol would have been unable to extract elements such as Al, K, Ca, Fe from complex silicate structures.[121–123] Higher extraction of Fe was found in literature when HNO_3 and hydrofluoric acid were used, indicating Fe was present in the particles as Fe-silicates.[27]

One of the most abundant types of particles on the TEM grids were organic carbon particles with inorganic inclusions (Fig. 9). These particles did not have distinct morphologies and instead clusters of particles appeared to be held in an organic matrix. The composition of the particles was predominantly C and O with minor elements such as Al, Fe, Na, and Co, which may exist in sulfate or chloride salts (see Fig. S-10 in the ESI†). The inorganic inclusions, and the fact that the particle organic matrix was unstable during exposure to the electron beam (Fig. 9) indicates that the particles were not tarballs or black carbon (aggregates of soot particles).

The crystallinity of the carbonaceous particles with a diameter greater than 1 μm can be semi-quantitatively evaluated using Raman spectroscopy. The G band (~1580 cm^{-1}) can be attributed to the stretching vibration mode with E_{2g} symmetry in the aromatic layers of the graphite crystalline, whilst the D_1 band at 1350 cm^{-1} is only active in the presence of disordered carbon and heteroatoms.[124–126] In perfect crystalline carbonaceous material only the G band is present in the first order

Open Access Article. Published on 20 January 2025. Downloaded on 3/14/2025 3:37:55 PM.
This article is licensed under a Creative Commons Attribution 3.0 Unported Licence.

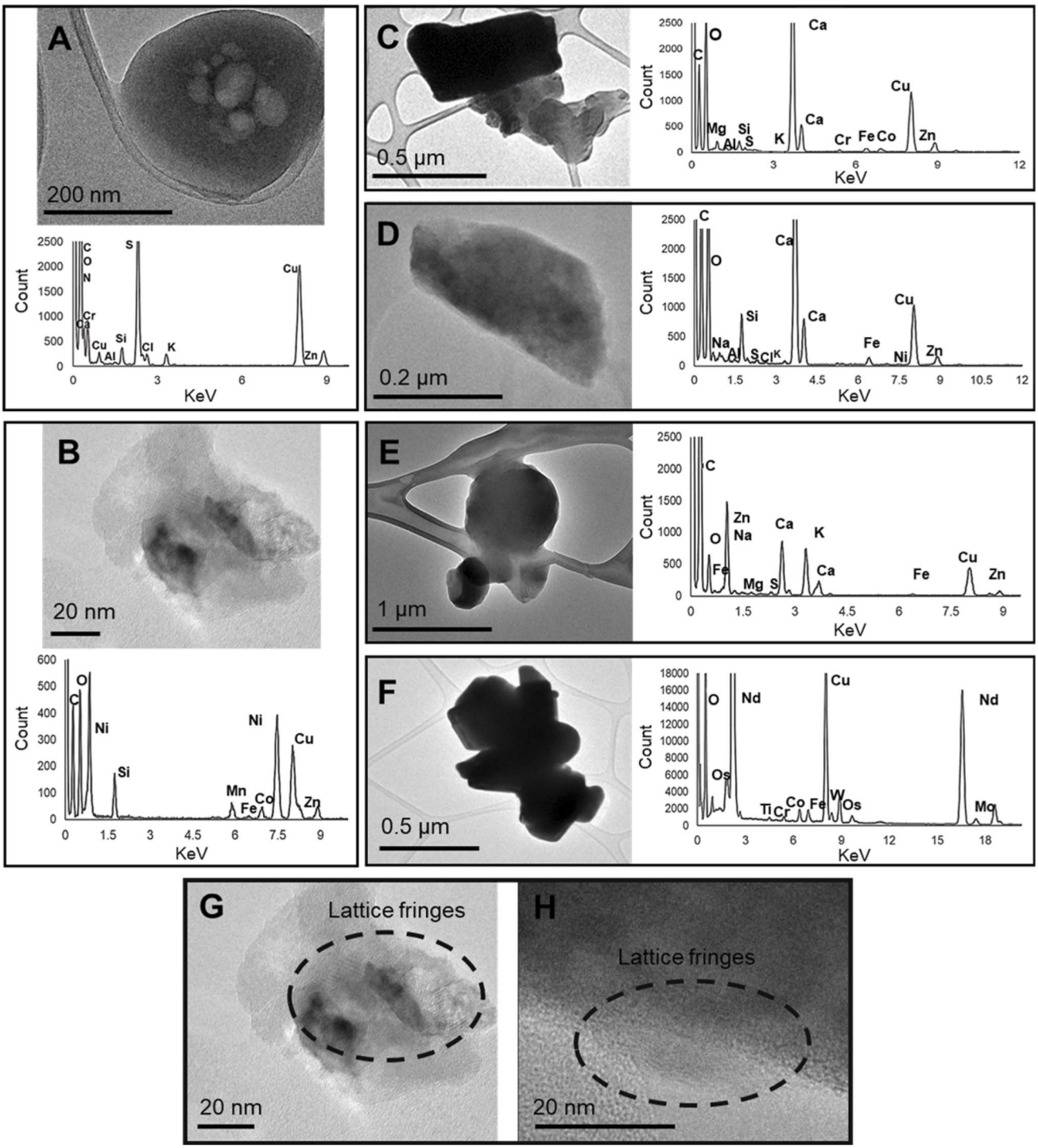

Fig. 8 TEM micrographs and EDS spectra for a range of different particles emitted from smouldering peat. The STEM-EDS maps of the particles are presented in Fig. S-4 to S-10 in the ESI.† C and Cu peaks also arise from the carbon film, copper TEM grids. Micrographs and EDS spectrum of: (A) a particle that contains a concentration of S and O, as well as other trace elements (Cr, Ca, Al, Si, Cl and K) and has a porous core; (B) a particle with a crystalline structure (lattice fringes shown in (G)) and consists of a high concentration of C, O and other trace elements (Ni, Si, Mn, Fe, Co, and Zn); (C) particles consisting of Ca, O and other trace elements (Na, Al, Si, S, Cl, K, Fe, Ni and Zn); (D) a particle with lattice fringes (shown in (H)) and consisting C, O and other trace elements (Ca, Fe, K, Mg, Na, S, and Zn); (E) a cluster of particles consisting of C, O, Fe, Zn, Na, Mg, S and Ca; (F) dense irregular particles held in an organic matrix, shown in Fig. S-8 in the ESI,† and consists of O, Os, Ti, Cr, Co, Fe Nd, Mo and W.

region.[126] The Raman spectra for the particles are shown in Fig. S-11 and S-12 in the ESI.† Both the D and G bands were present for the particles investigated, indicating the presence of amorphous carbon. This is supported by a broad peak between 1500 and 1600 cm^{-1}, as shown in Fig. S-12 in the ESI,† consistent with previous literature.[127] Comparatively, Fig. S-11

 © 2025 The Author(s). Published by the Royal Society of Chemistry

Open Access Article. Published on 20 January 2025. Downloaded on 3/14/2025 3:37:55 PM.
This article is licensed under a Creative Commons Attribution 3.0 Unported Licence.

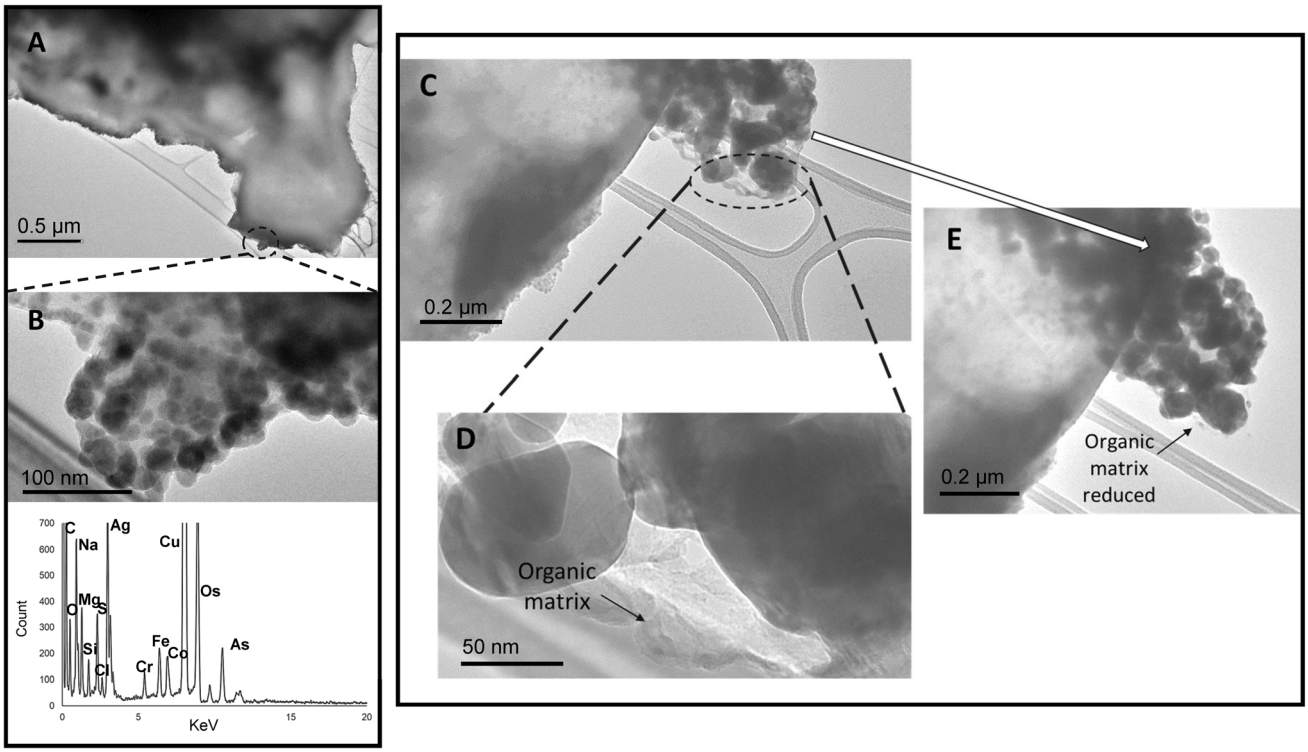

Fig. 9 TEM micrographs and EDS spectra of clusters of particles held in an organic matrix. The STEM-EDS maps of the particles are presented in Fig. S-10 in the ESI.† C and Cu peaks also arise are from the carbon film, copper TEM grids. Micrographs and EDS spectrum of: (A) a carbonaceous particles, (B) higher magnification image of the edge of the particle in (A) and corresponding EDS spectrum, (C) another region of the particle shown in (A), which shows a cluster of particles, (D) higher magnification image of the oval region in (C) showing it is made up of an organic matrix and particles, (E) same segment of particle shown in (C) after 5 minutes exposure to electron beam.

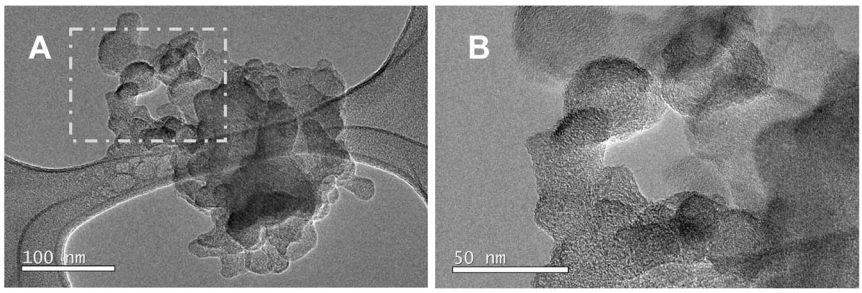

Fig. 10 Micrographs of a soot agglomerate identified on the TEM grid: (A) the entire soot agglomerate, and (B) graphitic layers within the soot agglomerate (top left corner of micrograph shown in (A)).

in the ESI† displays particles which have distinct D_1 and G bands. The D_1/G intensity ratio, known as the R_1 ratio,[128] was also calculated for the particles and presented in Table S-7 in the ESI.† The relative intensity of these bands provides a means of assessing the degree of crystallinity; the larger the R_1 ratio, the greater the amount of disordered carbon within the carbonaceous particles, whilst smaller ratio values alongside smaller full width at half maximum (FWMH) values indicate greater levels of graphitisation.[124] For ~80% of the particles analysed, the R_1 ratio indicated less graphitised carbon structures and greater levels of disorder.

Our TEM analysis found relatively few black carbon particles (*e.g.* Fig. 10), providing further evidence that black carbon does not make up a significant fraction of particles emitted from smouldering peat fires, in agreement with literature.[129] Flaming fires are known to emit greater levels of black carbon, in the form of soot aggregates.[113,130]

4 Implications

This study used the combination of aerodynamic and mobility diameter measurements for particle mass- and number-weighted concentrations. The average $PM_{2.5}$ mass

Open Access Article. Published on 20 January 2025. Downloaded on 3/14/2025 3:37:55 PM.
This article is licensed under a Creative Commons Attribution 3.0 Unported Licence.

concentration determined was greater than the 24 h mean air quality guideline values (15 μg m^{-3}) published by the WHO, whilst the *in situ* measured number-weighted particle concentration was two orders of magnitudes greater than the WHO's stated high 1 hour concentration (20 000 particles per cm^3). Fine and UFP can penetrate deeper in the respiratory system than coarse particles, and impact the respiratory system, heart rate variability, and cause mortality.[52,131] For example, literature has identified that the inhalation of UFP emitted from peat fires can decrease cardiac function and lead to a greater risk of a heart attack, whilst coarse particles can increase lung inflammation.[48] The comparisons of the aerodynamic and mobility diameter measurements further highlighted the importance of understanding the complex morphology, density, chemical composition, and dynamic nature of the particles emitted during wildfire events. OC was found to constitute 76% of the total particle mass. Greater levels of OC and polar organic compounds in biomass burning particles have been correlated with a higher oxidative potential.[132–134] Additionally, particle-bound carcinogenic PAHs have previously been found to constituted 0.1% of the total $PM_{2.5}$ OC mass.[17] The particle-bound PAHs in the peat fire emissions from this study will be reported elsewhere. Metals bound to the fine particle fraction can also be transported deep into the respiratory system and have been associated with adverse health effects.[29] For example, the uptake of redox active Fe in the body has been linked with hypertension, damage of tissues (such as liver, heart and joints) and neurological disorders such as Alzheimer's and Parkinson's disease,[76] whereas exposure to particle-bound Zn has also been correlated with inflammation, fibrosis, and pulmonary diseases.[135] Metal analysis by ICP-OES did not detect carcinogenic particle-bound Pb, and Ni, but TEM particle analysis identified metals such as Ni. The uptake of Ni, Cr(VI), and Cd in the respiratory system can lead to adverse health effects such as respiratory disorders, kidney damage, and DNA damage.[136] However, there are inconsistencies in the literature as to what contribution metals, such as Fe, Ni, Cr, Mn, and Zn make to the oxidative potential of the emitted particles and the health effects associated with the inhalation of the particles.[27,132] Consideration of dose, site of deposition, and bioavailability of the metals is important for toxicity studies.[29,137] However, the very high particle load during peatland fires, as well as redox active metals in the fine particle fraction provide a cause for concern for regional air quality and individuals, such as wildfire firefighters, who may be present in the immediate vicinity of the fires.[29]

Wildfire emission inventories and radiative forcing modelling also suffer from a limited number of particle EFs (mass- and number-weighted) and the possible underestimation of sources of brown carbon.[133] This study provides near-source number- and mass-weighted particle EFs, as well as specific chemical species EFs for smouldering-only peat fires. Consequently, this study builds on the limited number of temperate peat laboratory studies and provides greater understanding of how peat type and combustion dynamics can influence the release of particles, which could be applied to more complex field measurements and inform future atmospheric modelling work.

Furthermore, microscopy analysis found various Fe mineral phases. The partitioning of the mineral phases is important for assessing the light absorbing capacity of the particles and consequently the radiative effect of the particles emitted.[138–140] For example, the partitioning of goethite and hematite phases may be important for climate models because they are light absorbers in the shortwave spectrum.[138]

5 Conclusions

Simultaneous particle size distribution measurements, alongside offline chemical characterisation allowed for the size-resolved characterisation of particles emitted from smouldering peat fires. This included the evaluation of the *in situ* particle mass and number concentration, morphology, and chemical composition (organic carbon, elemental carbon, metals, and ionic species).

Particles with aerodynamic diameter of less than 2.5 μm contributed a significant proportion (94 ± 2%) of the total particle mass. Organic carbon accounted for 76% of the total particle mass, whilst microscopy and elemental carbon analysis provided only limited evidence of black carbon (<0.5% of total particle mass was elemental carbon). This provided further evidence that the optically active absorbing component of elemental carbon, black carbon, is not a major component of particles emitted from smouldering fires. Microscopy analysis identified an array of particle morphologies, including irregular shaped metal particles, spherical particles with sulfate chemistry, and organic matrix particles with internal particle clusters. Carcinogenic metals, such as Cd and Ni, were also present in some of the ultrafine particles. The size-resolved chemical analysis further found the fine particle fraction consisted of redox active metals such as Fe, as well as ionic species such as sulfate. As a result of the high *in situ* fine particle load, alongside 86% of the total metal mass residing in the smaller size fraction (less than 1 μm), exposure to the near source emissions could be a cause for concern for regional air quality and human health.

With the high risk and severity of smouldering peatland fires, especially in a warming climate, this study will inform research into the causal mechanisms that lead to adverse health effects if the particles are inhaled, as well as the particles direct and indirect climate forcing. Further research is required to investigate the variability in the size-resolved particle physicochemical characteristics and toxicity from a variety of smouldering fires as a function of plume age. Additionally, further work is required to characterise mineral phase partitioning, direct radiative effects, and cloud condensation nuclei activity.

Data availability

Data for this article, including microscopy spectral data files, Raman spectroscopy data files, particle mass, number and feret diameter size distribution data files, and particle-bound metal and ion concentration and emission factor data files are provided as ESI.†

 © 2025 The Author(s). Published by the Royal Society of Chemistry

Open Access Article. Published on 20 January 2025. Downloaded on 3/14/2025 3:37:55 PM.
This article is licensed under a Creative Commons Attribution 3.0 Unported Licence.

Author contributions

ALW: conceptualisation, methodology, investigation, writing – original draft, and visualisation. WC: methodology, investigation, and writing – review & editing. YH: methodology, investigation, and writing – review & editing. MC: investigation, writing – review & editing. GR: conceptualisation, methodology, resources, writing – review & editing, supervision, and funding acquisition. AEP: resources, and writing – review & editing. GF: resources, writing – review & editing, and supervision. MEJS: conceptualisation, methodology, resources, writing – review & editing, supervision, and funding acquisition.

Conflicts of interest

The authors declare that they have no conflict of interest.

Acknowledgements

This research was funded by the EPSRC Centre for Doctoral Training in Sustainable Civil Engineering grant (EP/L016826/1) and supported by the EPSRC Capital Award for Core Equipment (EP/T024712/1), as well as the ERC HAZE grant (682587). The authors would like to thank David Butterfield (National Physical Laboratory) for investigating the particles' OC/EC content and Mohsen Kazemimanesh and Adam Boies (University of Cambridge) for the supply of the thermophoretic sampler and advice on TEM analysis. Further thanks to Tom Smith (London School of Economics) and Gareth Clay (University of Manchester) for valuable discussions.

References

1 O. Hoegh-Guldberg, D. Jacob, M. Taylor, M. Bindi, S. Brown, I. Camilloni, A. Diedhiou, R. Djalante, K. L. Ebi, F. Engelbrecht, J. Guiot, Y. Hijioka, S. Mehrotra, A. Payne, S. I. Seneviratne, A. Thomas, R. Warren and G. Zhou, *Impacts of 1.5 °C Global Warming on Natural and Human Systems*, IPCC, 2018.
2 Y. Liu, J. Stanturf and S. Goodrick, Trends in global wildfire potential in a changing climate, *For. Ecol. Manage.*, 2010, **259**, 685–697.
3 X. Wang, D. K. Thompson, G. A. Marshall, C. Tymstra, R. Carr and M. D. Flannigan, Increasing frequency of extreme fire weather in Canada with climate change, *Clim. Change*, 2015, **130**, 573–586.
4 United Nations Environment Programme, *Emissions Gap Report 2020*, Nairobi, 2020.
5 D. Blake, A. L. Hinwood and P. Horwitz, Peat fires and air quality: Volatile organic compounds and particulates, *Chemosphere*, 2009, **76**, 419–423.
6 M. R. Turetsky, B. Benscoter, S. Page, G. Rein, G. R. Van Der Werf and A. Watts, Global vulnerability of peatlands to fire and carbon loss, *Nat. Geosci.*, 2014, **8**, 11–14.
7 G. Rein, Smouldering Fires and Natural Fuels, in *Fire Phenomena and the Earth System: an Interdisciplinary Guide to Fire Science*, ed. C. M. Belcher, Wiley and Sons, 2013, pp. 15–34.
8 J. Xu, P. J. Morris, J. Liu and J. Holden, PEATMAP: Refining estimates of global peatland distribution based on a meta-analysis, *Catena*, 2018, **160**, 134–140.
9 G. Rein, S. Cohen and A. Simeoni, Carbon emissions from smouldering peat in shallow and strong fronts, *Proc. Combust. Inst.*, 2009, **32**, 2489–2496.
10 R. Parish, A. Sirin, D. Charman, H. Joosten, T. Minayeva, M. Silvius and L. Stringer, *Assessment on Peatlands, Biodiversity and Climate Change: Main Report*, Global Environmental Centre, Kuala Lumpar, Wetlands International, Wageningen, 2008, vol. 1, pp. 1-37.
11 K. N. Palmer, Smouldering combustion in dusts and fibrous materials, *Combust. Flame*, 1957, **1**, 129–154.
12 G. Rein, N. Cleaver, C. Ashton, P. Pironi and J. L. Torero, The severity of smouldering peat fires and damage to the forest soil, *Catena*, 2008, **74**, 304–309.
13 D. Drysdale, *An Introduction to Fire Dynamics*, John Wiley & Sons, Ltd, 3rd edn, 2011.
14 IPCC, *Climate Change 2013: the Physical Science Basis*, Cambridge University Press, Cambridge, 2013.
15 Y. Hu, N. Fernandez-Anez, T. E. L. Smith and G. Rein, Review of emissions from smouldering peat fires and their contribution to regional haze episodes, *Int. J. Wildland Fire*, 2018, **27**, 293–312.
16 V. Samburova, J. Connolly, M. Gyawali, R. L. N. Yatavelli, A. C. Watts, R. K. Chakrabarty, B. Zielinska, H. Moosmüller and A. Khlystov, Polycyclic aromatic hydrocarbons in biomass-burning emissions and their contribution to light absorption and aerosol toxicity, *Sci. Total Environ.*, 2016, **568**, 391–401.
17 I. J. George, R. R. Black, C. D. Geron, J. Aurell, W. T. Preston and B. K. Gullett, Volatile and semivolatile organic compounds in laboratory peat fire emissions, *Atmos. Environ.*, 2016, **132**, 163–170.
18 Y. Hu, E. Christensen, F. Restuccia and G. Rein, Transient gas and particle emissions from smouldering combustion of peat, *Proc. Combust. Inst.*, 2019, **37**, 4035–4042.
19 B. Poulter, N. L. Christensen and P. N. Halpin, Carbon emissions from a temperate peat fire and its relevance to interannual variability of trace atmospheric greenhouse gases, *J. Geophys. Res.:Atmos.*, 2006, **111**, 1–11.
20 A. Hooijer, S. Page, J. G. Canadell, M. Silvius, J. Kwadijk, H. Wösten and J. Jauhiainen, Current and future CO2 emissions from drained peatlands in Southeast Asia, *Biogeosciences*, 2010, **7**, 1505–1514.
21 M. J. Wooster, D. L. A. Gaveau, M. A. Salim, T. Zhang, W. Xu, D. C. Green, V. Huijnen, D. Murdiyarso, D. Gunawan, N. Borchard, M. Schirrmann, B. Main and A. Sepriando, New tropical peatland gas and particulate emissions factors indicate 2015 Indonesian fires released far more particulate matter (but Less Methane) than current inventories imply, *Remote Sens.*, 2018, **10**, 1–31.
22 C. E. Stockwell, T. Jayarathne, M. A. Cochrane, K. C. Ryan, E. I. Putra, B. H. Saharjo, A. D. Nurhayati, I. Albar, D. R. Blake, I. J. Simpson, E. A. Stone and R. J. Yokelson,

Open Access Article. Published on 20 January 2025. Downloaded on 3/14/2025 3:37:55 PM.
This article is licensed under a Creative Commons Attribution 3.0 Unported Licence.

Field measurements of trace gases and aerosols emitted by peat fires in Central Kalimantan, Indonesia, during the 2015 El Niño, *Atmos. Chem. Phys.*, 2016, **16**, 11711–11732.

23 T. Jayarathne, C. E. Stockwell, R. J. Yokelson, S. Nakao and E. A. Stone, Emissions of Fine Particle Fluoride from Biomass Burning, *Environ. Sci. Technol.*, 2014, **48**, 12636–12644.

24 T. Jayarathne, C. E. Stockwell, A. Gilbert, K. Daugherty, M. Cochrane, K. Ryan, E. Putra, B. Saharjo, A. Nurhayati, I. Albar, R. Yokelson and E. A. Stone, Chemical characterisation of fine particulate matter emitted by peat fires in Central Kalimantan, Indonesia, during the 2015 El Nino, *Atmos. Chem. Phys.*, 2018, **18**, 2585–2600.

25 C. Geron and M. Hays, Air emissions from organic soil burning on the coastal plain of North Carolina, *Atmos. Environ.*, 2013, **64**, 192–199.

26 C. Roulston, C. Paton-Walsh, T. E. L. Smith, É.-A. Guérette, S. Evers, C. M. Yule, G. Rein and G. R. van der Werf, Fine particle emissions from tropical peat fires decrease rapidly with time since ignition, *J. Geophys. Res.:Atmos.*, 2018, **123**, 1–11.

27 R. Betha, S. N. Behera and R. Balasubramanian, 2013 Southeast Asian Smoke Haze: Fractionation of Particulate-Bound Elements and Associated Health Risk, *Environ. Sci. Technol.*, 2014, **48**, 4327–4335.

28 R. Betha, Z. Zhang and R. Balasubramanian, Influence of trans-boundary biomass burning impacted air masses on submicron particle number concentrations and size distributions, *Atmos. Environ.*, 2014, **92**, 9–18.

29 R. Betha, M. Pradani, P. Lestari, U. M. Joshi, J. S. Reid and R. Balasubramanian, Chemical speciation of trace metals emitted from Indonesian peat fires for health risk assessment, *Atmos. Res.*, 2013, **122**, 571–578.

30 Y. Fujii, W. Iriana, M. Oda, A. Puriwigati, S. Tohno, P. Lestari, A. Mizohata and H. S. Huboyo, Characteristics of carbonaceous aerosols emitted from peatland fire in Riau, Sumatra, Indonesia, *Atmos. Environ.*, 2014, **87**, 164–169.

31 Y. Fujii, S. Tohno, N. Amil, M. T. Latif, M. Oda, J. Matsumoto and A. Mizohata, Annual variations of carbonaceous PM2.5 in Malaysia: Influence by Indonesian peatland fires, *Atmos. Chem. Phys.*, 2015, **15**, 13319–13329.

32 R. R. Black, J. Aurell, A. Holder, I. J. George, B. K. Gullett, M. D. Hays, C. D. Geron and D. Tabor, Characterization of gas and particle emissions from laboratory burns of peat, *Atmos. Environ.*, 2016, **132**, 49–57.

33 Y. Iinuma, E. Brüggemann, T. Gnauk, K. Müller, M. O. Andreae, G. Helas, R. Parmar and H. Herrmann, Source characterization of biomass burning particles: The combustion of selected European conifers, African hardwood, savanna grass, and German and Indonesian peat, *J. Geophys. Res.*, 2007, **112**, 1–26.

34 A. A. May, G. R. McMeeking, T. Lee, J. W. Taylor, J. S. Craven, I. Burling, A. P. Sullivan, S. Akagi, J. L. Collett, M. Flynn, H. Coe, S. P. Urbanski, J. H. Seinfeld, R. J. Yokelson and S. M. Kreidenweis, Aerosol emissions from prescribed fires in the United States: A synthesis of laboratory and aircraft measurements, *J. Geophys. Res.:Atmos.*, 2014, **119**, 11826–11849.

35 P. Lestari, F. Muthmainnah and D. A. Permadi, Characterization of carbonaceous compounds emitted from Indonesian surface and sub surface peat burning, *Atmos. Pollut. Res.*, 2020, **11**, 1465–1472.

36 J. G. Watson, J. Cao, A. Chen, Q. Wang, J. Tian, S. Gronstal, S. S. H. Ho, A. C. Watts and J. C. Chow, Gaseous, PM 2.5 Mass, and Speciated Emission Factors from Laboratory Chamber Peat Combustion, *Atmos. Chem. Phys.*, 2019, **19**, 14173–14193.

37 C. Bhattarai, V. Samburova, D. Sengupta, M. Iaukea-Lum, A. C. Watts, H. Moosmüller and A. Y. Khlystov, Physical and chemical characterization of aerosol in fresh and aged emissions from open combustion of biomass fuels, *Aerosol Sci. Technol.*, 2018, **52**, 1266–1282.

38 A. G. Rappold, S. L. Stone, W. E. Cascio, L. M. Neas, V. J. Kilaru, M. S. Carraway, J. J. Szykman, A. Ising, W. E. Cleve, J. T. Meredith, H. Vaughan-Batten, L. Deyneka and R. B. Devlin, Peat Bog Wildfire Smoke Exposure in Rural North Carolina Is Associated with Cardiopulmonary Emergency Department Visits Assessed through Syndromic Surveillance, *Environ. Health Perspect.*, 2011, **119**, 1415–1420.

39 T. Sigsgaard, B. Forsberg, I. Annesi-Maesano, A. Blomberg, A. Bølling, C. Boman, J. Bønløkke, M. Brauer, N. Bruce, M.-E. Héroux, M.-R. Hirvonen, F. Kelly, N. Künzli, B. Lundbäck, H. Moshammer, C. Noonan, J. Pagels, G. Sallsten, J.-P. Sculier and B. Brunekreef, Health impacts of anthropogenic biomass burning in the developed world, *Eur. Respir. J.*, 2015, **46**, 1577–1588.

40 H. Youssouf, C. Liousse, L. Roblou, E.-M. Assamoi, R. O. Salonen, C. Maesano, S. Banerjee and I. Annesi-Maesano, Non-accidental health impacts of wildfire smoke, *Int. J. Environ. Res. Public Health*, 2014, **11**, 11772–11804.

41 S. K. Akagi, R. J. Yokelson, C. Wiedinmyer, M. J. Alvarado, J. S. Reid, T. Karl, J. D. Crounse and P. O. Wennberg, Emission factors for open and domestic biomass burning for use in atmospheric models, *Atmos. Chem. Phys.*, 2011, **11**, 4039–4072.

42 X. Huang and G. Rein, Smouldering combustion of peat in wildfires: Inverse modelling of the drying and the thermal and oxidative decomposition kinetics, *Combust. Flame*, 2014, **161**, 1633–1644.

43 X. Huang and G. Rein, Downward spread of smouldering peat fire: the role of moisture, density and oxygen supply, *Int. J. Wildland Fire*, 2017, **26**, 907–918.

44 W. Cui, Y. Hu and G. Rein, Experimental study of the ignition conditions for self-sustained smouldering in peat, *Proc. Combust. Inst.*, 2023, **39**, 4125–4133.

45 Y. Hu, W. Cui and G. Rein, Haze emissions from smouldering peat: The roles of inorganic content and bulk density, *Fire Saf. J.*, 2020, **113**, 102940.

46 X. Huang, F. Restuccia, M. Gramola and G. Rein, Experimental study of the formation and collapse of an

 © 2025 The Author(s). Published by the Royal Society of Chemistry

Open Access Article. Published on 20 January 2025. Downloaded on 3/14/2025 3:37:55 PM.
This article is licensed under a Creative Commons Attribution 3.0 Unported Licence.

overhang in the lateral spread of smouldering peat fires, *Combust. Flame*, 2016, **168**, 393–402.

47 Y. Hu, E. G. Christensen, H. M. F. Amin, T. E. L. Smith and G. Rein, Experimental study of moisture content effects on the transient gas and particle emissions from peat fires, *Combust. Flame*, 2019, **209**, 408–417.

48 Y. H. Kim, H. Tong, M. Daniels, E. Boykin, Q. Todd Krantz, J. McGee, M. Hays, K. Kovalcik, J. A. Dye and M. I. Gilmour, Cardiopulmonary toxicity of peat wildfire particulate matter and the predictive utility of precision cut lung slices, *Part. Fibre Toxicol.*, 2014, **11**, 1–17.

49 P. I. Jalava, R. O. Salonen, A. I. Hälinen, P. Penttinen, A. S. Pennanen, M. Sillanpää, E. Sandell, R. Hillamo and M. R. Hirvonen, In vitro inflammatory and cytotoxic effects of size-segregated particulate samples collected during long-range transport of wildfire smoke to Helsinki, *Toxicol. Appl. Pharmacol.*, 2006, **215**, 341–353.

50 C. A. Pope, R. T. Burnett, M. J. Thun, E. E. Calle, D. Krewski and G. D. Thurston, Lung Cancer, Cardiopulmonary Mortality, and Long-term Exposure to Fine Particulate Air Pollution, *JAMA, J. Am. Med. Assoc.*, 2002, **287**, 1132–1141.

51 R. W. Baldauf, R. B. Devlin, P. Gehr, R. Giannelli, B. Hassett-Sipple, H. Jung, G. Martini, J. McDonald, J. D. Sacks and K. Walker, Ultrafine Particle Metrics and Research Considerations: Review of the 2015 UFP Workshop, *Int. J. Environ. Res. Public Health*, 2016, **13**, 1–21.

52 S. C. Emmanuel, Impact to lung health of haze from forest fires: The Singapore experience, *Respirology*, 2000, **5**, 175–182.

53 J. S. Brown, K. L. Zeman and W. D. Bennett, Ultrafine Particle Deposition and Clearance in the Healthy and Obstructed Lung, *Am. J. Respir. Crit. Care Med.*, 2002, **166**, 1240–1247.

54 K. Donaldson, V. Stone, P. S. Gilmour, D. M. Brown and W. Macnee, Ultrafine Particles: Mechanisms of Lung Injury, *Philos. Trans. R. Soc. London*, 2000, **358**, 2741–2749.

55 A. Seaton, W. MacNee, K. Donaldson and D. Godden, Particulate air pollution and acute health effects, *Lancet*, 1995, **345**, 176–178.

56 S. Lu, M. Feng, Z. Yao, A. Jing, Z. Yufang, M. Wu, G. Sheng, J. Fu, S. Yonemochi, J. Zhang, Q. Wang and K. Donaldson, Physicochemical characterization and cytotoxicity of ambient coarse, fine, and ultrafine particulate matters in Shanghai atmosphere, *Atmos. Environ.*, 2011, **45**, 736–744.

57 Y. H. Kim, S. H. Warren, Q. T. Krantz, C. King, R. Jaskot, W. T. Preston, B. J. George, M. D. Hays, M. S. Landis, M. Higuchi, D. M. Demarini and M. I. Gilmour, Mutagenicity and Lung Toxicity of Smoldering *vs.* Flaming Emissions from Various Biomass Fuels: Implications for Health Effects from Wildland Fires, *Environ. Health Perspect.*, 2018, **126**, 1–14.

58 L. W. A. Chen, H. Moosmüller, W. P. Arnott, J. C. Chow, J. G. Watson, R. A. Susott, R. E. Babbitt, C. E. Wold, E. N. Lincoln and M. H. Wei, Emissions from laboratory combustion of wildland fuels: Emission factors and source profiles, *Environ. Sci. Technol.*, 2007, **41**, 4317–4325.

59 P. I. Jalava, R. O. Salonen, K. Nuutinen, A. S. Pennanen, M. S. Happo, J. Tissari, A. Frey, R. Hillamo, J. Jokiniemi and M. R. Hirvonen, Effect of combustion condition on cytotoxic and inflammatory activity of residential wood combustion particles, *Atmos. Environ.*, 2010, **44**, 1691–1698.

60 J. Tissari, J. Lyyränen, K. Hytönen, O. Sippula, U. Tapper, A. Frey, K. Saarnio, A. S. Pennanen, R. Hillamo, R. O. Salonen, M. R. Hirvonen and J. Jokiniemi, Fine particle and gaseous emissions from normal and smouldering wood combustion in a conventional masonry heater, *Atmos. Environ.*, 2008, **42**, 7862–7873.

61 J. S. Reid, R. Koppmann, T. F. Eck and D. P. Eleuterio, A review of biomass burning emissions part II: intensive physical properties of biomass burning particles, *Atmos. Chem. Phys.*, 2005, **5**, 799–825.

62 S. W. See, R. Balasubramanian, E. Rianawati, S. Karthikeyan and D. G. Streets, Characterization and Source Apportionment of Particulate Matter < 2.5 μm in Sumatra, Indonesia, during a Recent Peat Fire Episode, *Environ. Sci. Technol.*, 2007, **41**, 3488–3494.

63 A. Y. P. Wardoyo, L. Morawska, Z. D. Ristovski and J. Marsh, Quantification of Particle Number and Mass Emission Factors from Combustion of Queensland Trees, *Environ. Sci. Technol.*, 2006, **40**, 5696–5703.

64 H. D. Price, B. Stahlmecke, R. Arthur, H. Kaminski, J. Lindermann, E. Däuber, C. Asbach, T. A. J. Kuhlbusch, K. A. BéruBé and T. P. Jones, Comparison of instruments for particle number size distribution measurements in air quality monitoring, *J. Aerosol Sci.*, 2014, **76**, 48–55.

65 M. Marjamak, J. Keskinen, D.-R. Chen and D. Y. H. Pui, Performance evaluation of the Electrical Low-Pressure Impactor (ELPI), *J. Aerosol Sci.*, 2000, **31**, 249–261.

66 J. Leskinen, J. Joutsensaari, J. Lyyränen, J. Koivisto, J. Ruusunen, M. Järvelä, T. Tuomi, K. Hämeri, A. Auvinen and J. Jokiniemi, Comparison of nanoparticle measurement instruments for occupational health applications, *J. Nanopart. Res.*, 2012, **14**, 2–16.

67 A. Virtanen, M. Marjamäki, J. Ristimäki and J. Keskinen, Fine particle losses in electrical low-pressure impactor, *J. Aerosol Sci.*, 2001, **32**, 389–401.

68 J. F. P. Cornette, T. Coppieters, D. Desagher, J. Annendijck, H. Lepaumier, N. Faniel, I. Dyakov, J. Blondeau and S. Bram, Influence of the Dilution System and Electrical Low Pressure Impactor Performance on Particulate Emission Measurements from a Medium-scale Biomass Boiler, *Aerosol Air Qual. Res.*, 2020, **20**, 499–519.

69 WHO, *WHO Global Air Quality Guidelines: Particulate Matter (PM2.5 and PM10), Ozone, Nitrogen Dioxide, Sulfur Dioxide and Carbon Monoxide*, World Health Organization, Geneva, 2021.

70 G. Oberdörster, Z. Sharp, V. Atudorei, A. Elder, R. Gelein, W. Kreyling and C. Cox, Translocation of Inhaled Ultrafine Particles to the Brain, *Inhalation Toxicol.*, 2004, **16**, 437–445.

71 J. C. Chow, J. Cao, L.-W. A. Chen, X. Wang, Q. Wang, J. Tian, S. Sai, H. Ho, A. C. Watts, T. B. Carlson, S. D. Kohl and J. G. Watson, Changes in PM2.5 peat combustion source

Open Access Article. Published on 20 January 2025. Downloaded on 3/14/2025 3:37:55 PM.
This article is licensed under a Creative Commons Attribution 3.0 Unported Licence.

profiles with atmospheric aging in an oxidation flow reactor, *Atmos. Meas. Tech.*, 2019, **12**, 5475–5501.

72 Y. Fujii, H. Kawamoto, S. Tohno, M. Oda, W. Iriana and P. Lestari, Characteristics of carbonaceous aerosols emitted from peatland fire in Riau, Sumatra, Indonesia (2): Identification of organic compounds, *Atmos. Environ.*, 2015, **110**, 1–7.

73 O. Popovicheva, M. Kistler, E. Kireeva, N. Persiantseva, M. Timofeev, V. Kopeikin and A. Kasper-Giebl, Physicochemical characterization of smoke aerosol during large-scale wildfires: Extreme event of August 2010 in Moscow, *Atmos. Environ.*, 2014, **96**, 405–414.

74 K. R. Smith, J. M. Veranth, A. A. Hu, J. A. S. Lighty and A. E. Aust, Interleukin-8 Levels in Human Lung Epithelial Cells Are Increased in Response to Coal Fly Ash and Vary with the Bioavailability of Iron, as a Function of Particle Size and Source of Coal, *Chem. Res. Toxicol.*, 2000, **13**, 118–125.

75 M. B. Kadiiska, R. P. Mason, K. L. Dreher, D. L. Costa and A. J. Ghio, In Vivo Evidence of Free Radical Formation in the Rat Lung after Exposure to an Emission Source Air Pollution Particle, *Chem. Res. Toxicol.*, 1997, **10**, 1104–1108.

76 K. Jomova, S. Baros and M. Valko, Redox active metal-induced oxidative stress in biological systems, *Transition Met. Chem.*, 2012, **37**, 127–134.

77 X. Huang, R. Betha, L. Y. Tan and R. Balasubramanian, Risk assessment of bioaccessible trace elements in smoke haze aerosols *versus* urban aerosols using simulated lung fluids, *Atmos. Environ.*, 2016, **125**, 505–511.

78 O. S. Usmani, M. F. Biddiscombe and P. J. Barnes, Regional Lung Deposition and Bronchodilator Response as a Function of β2-Agonist Particle Size, *Am. J. Respir. Crit. Care Med.*, 2005, **172**, 1497–1504.

79 J. S. Lighty, J. M. Veranth and A. F. Sarofim, Combustion Aerosols: Factors Governing Their Size and Composition and Implications to Human Health, *J. Air Waste Manage. Assoc.*, 2000, **50**, 1565–1618.

80 W. G. Kreyling, M. Semmler-Behnke and W. Möller, Ultrafine Particle-Lung Interactions: Does Size Matter?, *J. Aerosol Med.*, 2006, **19**, 74–83.

81 E. Christensen, Y. Hu, F. Restuccia, M. A. Santoso, X. Huang and G. Rein, Experimental methods and scales in smouldering wildfires, in *Fire Effects on Soil Properties*, ed. P. Pereira, J. Mataix-Solera, X. Úbeda, G. Rein and A. Cerdà, CSIRO Publishing, 2019, pp. 267–280.

82 A. Usup, Y. Hashimoto, H. Takahashi and H. Hayasaka, Combustion and thermal characteristics of peat fire in tropical peatland in Central Kalimantan, Indonesia, *Tropics*, 2004, **14**, 1–19.

83 W. Cui, *Laboratory investigation of the ignition and spread of smouldering in peat samples of different origins and the associated emissions*, Imperial College London, 2022.

84 W. Cui, S. Dossi and G. Rein, Laboratory benchmark of low-cost portable gas and particle analysers at the source of smouldering wildfires, *Int. J. Wildland Fire*, 2023, **32**, 1542–1557.

85 P. A. Baron, P. Kulkarni and K. Willeke, *Particle Measurement: Principles, Techniques, and Applications*, John Wiley & Sons, Inc., 3rd edn, 2011.

86 M. Kazemimanesh, R. Dastanpour, A. Baldelli, A. Moallemi, K. A. Thomson, M. A. Jefferson, M. R. Johnson, S. N. Rogak and J. S. Olfert, Size, effective density, morphology, and nano-structure of soot particles generated from buoyant turbulent diffusion flames, *J. Aerosol Sci.*, 2019, **132**, 22–31.

87 S. Karthikeyan, U. M. Joshi and R. Balasubramanian, Microwave assisted sample preparation for determining water-soluble fraction of trace elements in urban airborne particulate matter: Evaluation of bioavailability, *Anal. Chim. Acta*, 2006, **576**, 23–30.

88 R. J. Yokelson, J. G. Goode, D. E. Ward, R. A. Susott, R. E. Babbitt, D. D. Wade, I. Bertschi, D. W. T. Griffith and W. M. Hao, Emissions of formaldehyde, acetic acid, methanol, and other trace gases from biomass fires in North Carolina measured by airborne Fourier transform infrared spectroscopy, *J. Geophys. Res.*, 1999, **104**, 30109–30125.

89 R. Delmas, J. P. Lacaux and D. Brocard, Determination of biomass burning emission factors: methods and results, *Environ. Monit. Assess.*, 1995, **38**, 181–204.

90 O. B. Popovicheva, E. Guenter, I.-T. Ku, M. A. Timofeev and N. K. Shonija, Aerosol Emissions from Long-lasting Smoldering of Boreal Peatlands: Chemical Composition, Markers, and Microstructure, *Aerosol Air Qual. Res.*, 2019, **19**, 484–503.

91 G. Engling, J. He, R. Betha and R. Balasubramanian, Assessing the regional impact of indonesian biomass burning emissions based on organic molecular tracers and chemical mass balance modeling, *Atmos. Chem. Phys.*, 2014, **14**, 8043–8054.

92 S. W. See, R. Balasubramanian and W. Wang, A study of the physical, chemical, and optical properties of ambient aerosol particles in Southeast Asia during hazy and nonhazy days, *J. Geophys. Res.*, 2006, **111**, 1–12.

93 F. Reisen, C. P. Meyer, C. J. Weston and L. Volkova, Ground-Based Field Measurements of PM 2.5 Emission Factors From Flaming and Smoldering Combustion in Eucalypt Forests, *J. Geophys. Res.:Atmos.*, 2018, **123**, 8301–8314.

94 S. Simões Amaral, J. Andrade De Carvalho, M. Angélica Martins Costa and C. Pinheiro, An Overview of Particulate Matter Measurement Instruments, *Atmosphere*, 2015, **6**, 1327–1345.

95 M. M. Maricq, D. H. Podsiadlik and R. E. Chase, Size Distributions of Motor Vehicle Exhaust PM: A Comparison Between ELPI and SMPS Measurements, *Aerosol Sci. Technol.*, 2000, **33**, 239–260.

96 I. T. Kero and R. B. Jørgensen, Comparison of Three Real-Time Measurement Methods for Airborne Ultrafine Particles in the Silicon Alloy Industry, *Int. J. Environ. Res. Public Health*, 2016, **13**, 1–14.

97 C. Van Gulijk, J. C. M. Marijnissen, M. Makkee, J. A. Moulijn and A. Schmidt-Ott, Measuring diesel soot with a scanning mobility particle sizer and an electrical low-pressure

 © 2025 The Author(s). Published by the Royal Society of Chemistry

Open Access Article. Published on 20 January 2025. Downloaded on 3/14/2025 3:37:55 PM.
This article is licensed under a Creative Commons Attribution 3.0 Unported Licence.

impactor: performance assessment with a model for fractal-like agglomerates, *J. Aerosol Sci.*, 2004, **35**, 633–655.

98 S. Janhäll, M. O. Andreae and U. Pöschl, Atmospheric Chemistry and Physics Biomass burning aerosol emissions from vegetation fires: particle number and mass emission factors and size distributions, *Atmos. Chem. Phys.*, 2010, **10**, 1427–1439.

99 J. Leskinen, J. Tissari, O. Uski, A. Virén, T. Torvela, T. Kaivosoja, H. Lamberg, I. Nuutinen, T. Kettunen, J. Joutsensaari, P. I. Jalava, O. Sippula, M. R. Hirvonen and J. Jokiniemi, Fine particle emissions in three different combustion conditions of a wood chip-fired appliance - Particulate physico-chemical properties and induced cell death, *Atmos. Environ.*, 2014, **86**, 129–139.

100 A. C. Kalogridis, O. B. Popovicheva, G. Engling, E. Diapouli, K. Kawamura, E. Tachibana, K. Ono, V. S. Kozlov and K. Eleftheriadis, Smoke aerosol chemistry and aging of Siberian biomass burning emissions in a large aerosol chamber, *Atmos. Environ.*, 2018, **185**, 15–28.

101 H. Wiinikka, C. Grönberg and C. Boman, Emissions of heavy metals during fixed-bed combustion of six biomass fuels, *Energy Fuels*, 2013, **27**, 1073–1080.

102 E. Gorham and J. A. Janssens, The distribution and accumulation of chemical elements in five peat cores from the mid-continent to the eastern coast of North America, *Wetlands*, 2005, **25**(2), 259–278.

103 R. Das, X. Wang, M. Itoh, S. Shiodera and M. Kuwata, Estimation of Metal Emissions From Tropical Peatland Burning in Indonesia by Controlled Laboratory Experiments, *J. Geophys. Res.:Atmos.*, 2019, **124**, 6583–6599.

104 M. Othman and M. T. Latif, Dust and gas emissions from small-scale peat combustion, *Aerosol Air Qual. Res.*, 2013, **13**, 1045–1059.

105 Y. H. Kim, C. King, T. Krantz, M. M. Hargrove, I. J. George, J. McGee, L. Copeland, M. D. Hays, M. S. Landis, M. Higuchi, S. H. Gavett and M. I. Gilmour, The role of fuel type and combustion phase on the toxicity of biomass smoke following inhalation exposure in mice, *Arch. Toxicol.*, 2019, **93**, 1501–1513.

106 M. Ahmed, X. Guo and X. M. Zhao, Determination and analysis of trace metals and surfactant in air particulate matter during biomass burning haze episode in Malaysia, *Atmos. Environ.*, 2016, **141**, 219–229.

107 M. Z. Akbari, D. Thepnuan, W. Wiriya, R. Janta, P. Pansompong, P. Hemwan, A. Charoenpanyanet and S. Chantara, Emission factors of metals bound with PM2.5 and ashes from biomass burning simulated in an open-system combustion chamber for estimation of open burning emissions, *Atmos. Pollut. Res.*, 2021, **12**, 13–24.

108 K. Kawamura and K. Ikushima, Seasonal Changes in the Distribution of Dicarboxylic Acids in the Urban Atmosphere, *Environ. Sci. Technol.*, 1993, **27**, 2227–2235.

109 K. Kawamura, H. Kasukabe and L. A. Barrie, Source and reaction pathways of dicarboxylic acids, ketoacids and dicarbonyls in Arctic aerosols: one year of observations, *Atmos. Environ.*, 1996, **30**, 1709–1722.

110 L. Wu, L. Wei, G. Wang and J. Zhao, Comparison of Atmospheric Monocarboxylic and Dicarboxylic Acids in Xi' an, China, for Source Apportionment of Organic Aerosols, *Water, Air, Soil Pollut.*, 2020, **231**, 337.

111 K. Adachi, A. J. Sedlacek, L. Kleinman, S. R. Springston, J. Wang, D. Chand, J. M. Hubbe, J. E. Shilling, T. B. Onasch, T. Kinase, K. Sakata, Y. Takahashi and P. R. Buseck, Spherical tarball particles form through rapid chemical and physical changes of organic matter in biomass-burning smoke, *Proc. Natl. Acad. Sci. U. S. A.*, 2019, **116**, 19336–19341.

112 Y. Liu, X. Meng, Z. Wu, D. Huang, H. Wang, J. Chen, J. Chen, T. Zong, X. Fang, T. Tan, G. Zhao, S. Chen, L. Zeng, S. Guo, X. Huang, L. He, L. Zeng and M. Hu, The particle phase state during the biomass burning events, *Sci. Total Environ.*, 2021, **792**, 1–6.

113 M. Pósfai, R. Simonics, J. Li, P. V Hobbs and P. R. Buseck, Individual aerosol particles from biomass burning in southern Africa: 1. Compositions and size distributions of carbonaceous particles, *J. Geophys. Res.*, 2003, **108**(D13), 1–13.

114 A. J. Sedlacek, P. R. Buseck, K. Adachi, T. B. Onasch, S. R. Springston and L. Kleinman, Formation and evolution of tar balls from northwestern US wildfires, *Atmos. Chem. Phys.*, 2018, **18**, 11289–11301.

115 E. Diapouli, O. Popovicheva, M. Kistler, S. Vratolis, N. Persiantseva, M. Timofeev, A. Kasper-Giebl and K. Eleftheriadis, Physicochemical characterization of aged biomass burning aerosol after long-range transport to Greece from large scale wildfires in Russia and surrounding regions, Summer 2010, *Atmos. Environ.*, 2014, **96**, 393–404.

116 C. K. McMahon, D. D. Wade and S. N. Tsoukalas, *Combustion Characteristics and Emissions from Burning Organic Soils, Annual Meeting of the Air Pollution*, Control Association, Montreal, 1980.

117 Y. Xie, A. Ding, W. Nie, H. Mao, X. Qi, X. Huang, Z. Xu, V. M. Kerminen, T. Petäjä, X. Chi, A. Virkkula, M. Boy, L. Xue, J. Guo, J. Sun, X. Yang, M. Kulmala and C. Fu, Enhanced sulfate formation by nitrogen dioxide: Implications from *in situ* observations at the SORPES station, *J. Geophys. Res.:Atmos.*, 2015, **120**, 12679–12694.

118 T. Liu and J. P. D. Abbatt, Oxidation of sulfur dioxide by nitrogen dioxide accelerated at the interface of deliquesced aerosol particles, *Nat. Chem.*, 2021, **13**(12), 1173–1177.

119 I. N. Sokolik, J. L. Rajot, S. Caquineau and A. Gaudichet, Characterization of iron oxides in mineral dust aerosols: Implications for light absorption, *J. Geophys. Res.*, 2006, **111**, 1–19.

120 S. Lafon, J. L. Rajot, S. C. Alfaro and A. Gaudichet, Quantification of iron oxides in desert aerosol, *Atmos. Environ.*, 2004, **38**, 1211–1218.

121 J. Li, M. Pósfai, P. V. Hobbs and P. R. Buseck, Individual aerosol particles from biomass burning in southern Africa: 2, Compositions and aging of inorganic particles, *J. Geophys. Res.:Atmos.*, 2003, **108**, 1–11.

Open Access Article. Published on 20 January 2025. Downloaded on 3/14/2025 3:37:55 PM.
This article is licensed under a Creative Commons Attribution 3.0 Unported Licence.

122 K. Swami, C. D. Judd, J. Orsini, K. X. Yang and L. Husain, Microwave assisted digestion of atmospheric aerosol samples followed by inductively coupled plasma mass spectrometry determination of trace elements, *Fresenius. J. Anal. Chem.*, 2001, **369**, 63–70.

123 H. Ormstad, P. I. Gaarder and B. V. Johansen, Quantification and characterisation of suspended particulate matter in indoor air, *Sci. Total Environ.*, 1997, **193**, 185–196.

124 S. K. Sze, N. Siddique, J. J. Sloan and R. Escribano, Raman spectroscopic characterization of carbonaceous aerosols, *Atmos. Environ.*, 2001, **35**, 561–568.

125 A. C. Ferrari and J. Robertson, Interpretation of Raman spectra of disordered and amorphous carbon, *Phys. Rev. B:Condens. Matter Mater. Phys.*, 2000, **61**, 14095–14107.

126 Y. Feng, L. Liu, Y. Yang, Y. Deng, K. Li, H. Cheng, X. Dong, W. Li and L. Zhang, The application of Raman spectroscopy combined with multivariable analysis on source apportionment of atmospheric black carbon aerosols, *Sci. Total Environ.*, 2019, **685**, 189–196.

127 D. R. Tallant, T. A. Friedmann, N. A. Missert, M. P. Siegal and J. P. Sullivan, Raman spectroscopy of amorphous carbon, *Mater. Res. Soc. Symp. Proc.*, 1997, **498**, 37–48.

128 O. Beyssac, B. Goffé, J. P. Petitet, E. Froigneux, M. Moreau and J. N. Rouzaud, On the characterization of disordered and heterogeneous carbonaceous materials by Raman spectroscopy, *Spectrochim. Acta, Part A*, 2003, **59**, 2267–2276.

129 R. K. Chakrabarty, M. Gyawali, R. L. N. Yatavelli, A. Pandey, A. C. Watts, J. Knue, L.-W. A. Chen, R. R. Pattison, A. Tsibart, V. Samburova and H. Moosmüller, Brown carbon aerosols from burning of boreal peatlands: microphysical properties, emission factors, and implications for direct radiative forcing, *Atmos. Chem. Phys.*, 2016, **16**, 3033–3040.

130 R. K. Chakrabarty, H. Moosmüller, M. A. Garro, W. P. Arnott, J. Walker, R. A. Susott, R. E. Babbitt, C. E. Wold, E. N. Lincoln and W. M. Hao, Emissions from the laboratory combustion of wildland fuels: Particle morphology and size, *J. Geophys. Res.:Atmos.*, 2006, **111**, 1–16.

131 P. Monks, J. Allan, D. Carruthers, D. Carslaw, G. Fuller, R. Harrison, M. Heal, A. Lewis, E. Nemitz, C. Reeves and M. Williams, *Ultrafine Particles (UFP) in the UK*, London, 2018.

132 A. Fushimi, K. Saitoh, K. Hayashi, K. Ono, Y. Fujitani, A. M. Villalobos, B. R. Shelton, A. Takami, K. Tanabe and J. J. Schauer, Chemical characterization and oxidative potential of particles emitted from open burning of cereal straws and rice husk under flaming and smoldering conditions, *Atmos. Environ.*, 2017, **163**, 118–127.

133 A. Arneth, H. Barbosa, T. Benton, K. Calvin, E. Calvo, S. Connors, A. Cowie, E. Davin, F. Denton, R. van Diemen, F. Driouech, A. Elbehri, J. Evans, M. Ferrat, J. Harold, E. Haughey, M. Herroro, J. House, E. Howden, M. Hurlbert, G. Jia, T. G. Johansen, J. Krishnaswamy, W. Kurz, C. Lennard, S. Myeong, N. Mahmoud, V. Masson-Delmotte, C. Mbow, P. McElwee, A. Mirzabaev, A. Morelli, W. Moufouma-Okia, D. Nedjraoui, S. Neogi, J. Nkem, N. Noblet-Ducoudré, L. Olsson, M. Pathak, J. Petzold, R. Pichs-Madruga, E. Poloczanska, A. Popp, A. Reisinger, D. C. Roberts, C. Rosenzweig, M. Rounsevell, E. Shevliakova, P. Shukla, J. Skea, R. Slade, P. Smith, Y. Sokona, D. Sonwa, J.-F. Soussana, F. Tubiello, L. Verchot, K. Warner, N. Weyer, J. Wu, N. Yassaa, P. Zhai and Z. Zommers, *IPCC Special Report on Climate Change, Desertification, Land Degradation, Sustainable Land Management, Food Security, and Greenhouse Gas Fluxes in Terrestrial Ecosystems*, 2019.

134 V. Verma, A. Polidori, J. J. Schauer, M. M. Shafer, F. R. Cassee and C. Sioutas, Physicochemical and toxicological profiles of particulate matter in Los Angeles during the October 2007 Southern California wildfires, *Environ. Sci. Technol.*, 2009, **43**, 954–960.

135 I. Y. R. Adamson, H. Prieditis, C. Hedgecock and R. Vincent, Zinc is the toxic factor in the lung response to an atmospheric particulate sample, *Toxicol. Appl. Pharmacol.*, 2000, **166**, 111–119.

136 S. J. Mulware, Trace elements and carcinogenicity: a subject in review, *Biotech*, 2013, **3**, 85–96.

137 L. C. Thompson, Y. H. Kim, B. L. Martin, A. D. Ledbetter, J. A. Dye, M. S. Hazari, M. I. Gilmour and A. K. Farraj, Pulmonary exposure to peat smoke extracts in rats decreases expiratory time and increases left heart end systolic volume, *Inhalation Toxicol.*, 2018, **30**, 439–447.

138 P. Formenti, S. Caquineau, S. Chevaillier, A. Klaver, K. Desboeufs, J. L. Rajot, S. Belin and V. Briois, Dominance of goethite over hematite in iron oxides of mineral dust from Western Africa: Quantitative partitioning by X-ray absorption spectroscopy, *J. Geophys. Res.:Atmos.*, 2014, **119**, 12740–12754.

139 X. L. Zhang, G. J. Wu, C. L. Zhang, T. L. Xu and Q. Q. Zhou, What is the real role of iron oxides in the optical properties of dust aerosols?, *Atmos. Chem. Phys.*, 2015, **15**, 12159–12177.

140 Y. Cudennec and A. Lecerf, The transformation of ferrihydrite into goethite or hematite, revisited, *J. Solid State Chem.*, 2006, **179**, 716–722.

 © 2025 The Author(s). Published by the Royal Society of Chemistry